Nonlocal Markovian models for image denoising

Denis H. P. Salvadeo
Nelson D. A. Mascarenhas
Alexandre L. M. Levada

Nonlocal Markovian models for image denoising

Denis H. P. Salvadeo,[a,b,*] **Nelson D. A. Mascarenhas,**[b,c] **and Alexandre L. M. Levada**[b]
[a]São Paulo State University, Department of Statistics, Applied Mathematics and Computation, Rua 24A, 1515, Rio Claro 13503-013, Brazil
[b]Federal University of São Carlos, Computing Department, Via Washington Luis, Km 235, São Carlos 13565-905, Brazil
[c]Faculdade Campo Limpo Paulista, Graduate Program in Computer Science, Rua Guatemala, 170, Campo Limpo Paulista 13231-230, Brazil

Abstract. Currently, the state-of-the art methods for image denoising are patch-based approaches. Redundant information present in nonlocal regions (patches) of the image is considered for better image modeling, resulting in an improved quality of filtering. In this respect, nonlocal Markov random field (MRF) models are proposed by redefining the energy functions of classical MRF models to adopt a nonlocal approach. With the new energy functions, the pairwise pixel interaction is weighted according to the similarities between the patches corresponding to each pair. Also, a maximum pseudolikelihood estimation of the spatial dependency parameter (β) for these models is presented here. For evaluating this proposal, these models are used as an *a priori* model in a maximum *a posteriori* estimation to denoise additive white Gaussian noise in images. Finally, results display a notable improvement in both quantitative and qualitative terms in comparison with the local MRFs. © *2016 SPIE and IS&T* [DOI: 10.1117/1.JEI.25.1.013003]

1 Introduction

Suitable image modeling can provide great advances to solve problems in image processing.[1] One of these problems is image denoising, which is a basic step for many applications in image processing and analysis. However, despite the important advances achieved in the last 10 years, this problem is still open.[2]

Historically, the Wiener filter[3] is the traditional method to denoise images. It is the optimum filter in the sense of linear minimum mean square error (MSE) estimation. The 90s were a very productive decade for image denoising proposals, with four approaches emerging as solutions for this problem,[4,5] as well as several posterior combinations of them: anisotropic diffusion,[6–9] total variation,[10,11] wavelets,[12] and bilateral filtering.[13,14]

Anisotropic diffusion is a multiscale technique based on partial differential equations for a heat diffusion equation, where the diffusion coefficient is a function of the image gradient.[6] Thus, the idea is to convolve the image with Gaussian kernels on various scales (variances) to obtain blurred images in several resolutions but with smoothing controlled according to the probability of a pixel being a boundary region, causing an effect of reduction or stopping of the diffusion process on edge regions (edges are less smoothed).[6]

Total variation for image denoising was introduced by Ref. 10. Basically, this approach defines the denoising problem as an optimization process to estimate the free-noise image that minimizes the MSE with a regularization term defined in terms of the integral of the magnitude of the image gradient (total variation).[10,11] In other words, defining the regularization parameter (λ) tending to infinity leads to smoothing the image (total variation tends to zero), but

preserving more edge regions (in the boundaries, the MSE is close to zero).

In turn, image denoising by using wavelets was first proposed by Ref. 12, corresponding to wavelet shrinkage. In general, techniques in this approach apply a wavelet transform to obtain the coefficients in the sparse domain of wavelets by using a wavelet basis. In this domain, noise corrupts all coefficients only slightly, turning null coefficients to nonnull coefficients. Thus, according to a threshold T, smaller coefficients should be defined to zero, while larger coefficients are attenuated or remained unchanged. Basically, a key point here is to determine T.

A bilateral filter[13,14] estimates the noise-free pixel by an average mean of the neighbor pixels. In this approach, the weights are defined in terms of two local dissimilarities: spatial and radiometric differences among the central and their neighbor pixels.

Recently, in the last decade, techniques for two approaches have been proposed: nonlocal approaches[4,15] and compressive sensing.[16,17] In the first case, two techniques based on nonlocal approaches have been developed, corresponding to the state-of-art ones for image denoising: nonlocal means (NLM)[4] and block matching and three-dimensional filtering (BM3D).[15] Techniques in this approach model the redundant information in images for a better estimation of the noise-free pixel. More details, mainly about NLM, are discussed in the text. The latter, compressive sensing,[16,17] also defines a regularization problem, but it is now based on L1-minimization of the sparse coefficients.

Mathematically, the degradation, measurement model for the image denoising problem can be described by the following equation:

$$\vec{y} = \vec{z} + \vec{\eta}, \tag{1}$$

*Address all correspondence to: Denis Henrique Pinheiro Salvadeo, E-mail: salvadeo@rc.unesp.br
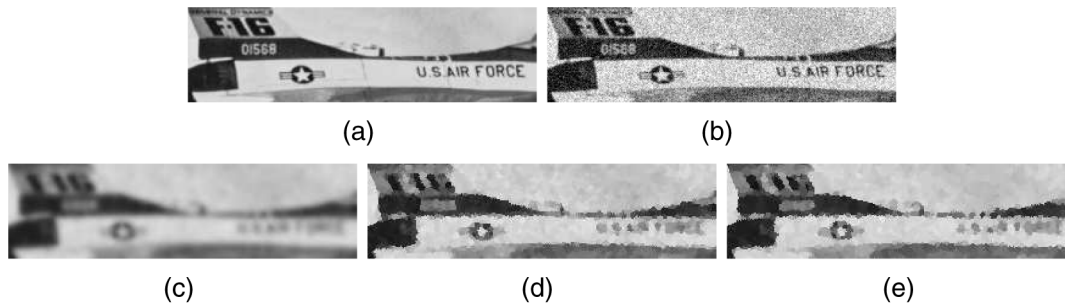
Fig. 1 Results for image denoising by using local Markov random field (MRF) priors (c)–(e) in a maximum *a posteriori* (MAP)-MRF framework: (a) original, (b) noisy, (c) Gaussian Markov random field (GMRF), (d) Potts, and (e) generalized multilevel logistic (GIMLL). Only a section of the classical Jet Plane image is shown.

where $\vec{y}$ is an observed noisy image, $\vec{z}$ is an original (noise-free) image to be estimated, and $\vec{\eta}$ is the noise.

A solution for this problem can be defined by adopting a maximum *a posteriori* (MAP) estimation criterion as

$$\hat{\vec{z}} = \max_z p(z|y) \propto \max_z p(y|z)p(z), \tag{2}$$

where $\hat{z}$ is an estimated noise-free image, $p(z|y)$ is the *a posteriori* probability density function, $p(y|z)$ is the likelihood, and $p(z)$ is an *a priori* probability density function.

This filtering process is an ill-posed inverse problem, such that constraints or other *a priori* knowledge are very important to restrict the solution by modeling the likelihood and *a priori* probability density functions. Among the characteristics that can be represented are sparsity, redundancy, noise, and spatial correlation between the pixels. Usually, the latter is modeled by Markov random fields (MRFs).[18] However, MRF models, such as Potts,[19] generalized multilevel logistic (GIMLL),[19] Gaussian Markov random field (GMRF), or autonormal,[19,20] tend to oversmooth the images or generate poor quality of edges, as can be noted in Fig. 1. These results are obtained by using these models in a MAP estimation (i.e., a MAP–MRF framework), as performed in Ref. 21.

Therefore, more suitable MRF models for image denoising problems are necessary. In this paper, we propose to extend classical MRF models by weighting the potential cliques in a nonlocal patch-based approach. In other words, these new models consist of a nonlocal Markov random field (NLMRF) approach. This improved modeling is in accordance with the proposals in the state-of-the art methods for image denoising,[22] such as NLM[4] and BM3D collaborative filtering.[15]

In the literature, several methods, such as those in Refs. 23–26, follow a NLMRF approach. Basically, Chen et al.[23,24] propose a nonlocal Markovian model for computed tomography and positron emission tomography reconstruction, respectively. In this model, the energy function is defined as a weighted sum of Euclidean distances between pixels in the field. However, fixed values were used for the spatial dependency parameter (β). In turn, Zhao et al.[25] propose a nonlocal Markovian model for satellite image deconvolution by weighting an L1-norm of differences between neighbor pixels and assuming the parameter β as a regularization term in an energy function to be minimized. An L-curve method was used to estimate this parameter. In Ref. 26, an NLMRF model based on a field of experts

was proposed for image restoration, mainly image denoising and inpainting problems, by using a gradient-based discrimination learning framework for training the model (the parameter β was not explicitly specified).

In the present paper, nonlocal patch-based versions for GMRF, Potts, and GIMLL, as well as their parameter estimation, are proposed. In case of nonlocal GMRF (NLGRMF), a closed formula was found to estimate the spatial dependency parameter (β) of the model. These new models were applied for image denoising problems to evaluate them.

This paper is organized as follows. In Sec. 2, the MRF theory is briefly described. In Sec. 3, the proposed models are specified in detail, and their parameter estimation by using a maximum pseudolikelihood estimation (MPLE) are presented in Sec. 4. Section 5 describes the methodology used for the proposal evaluation, and Sec. 6 displays and discusses the denoising results. Finally, conclusions and future works are presented in Sec. 7.

2 Markov Random Fields

MRFs can be understood based on the following idea in statistical mechanics to characterize the total energy between particle interactions systems: the contribution of each
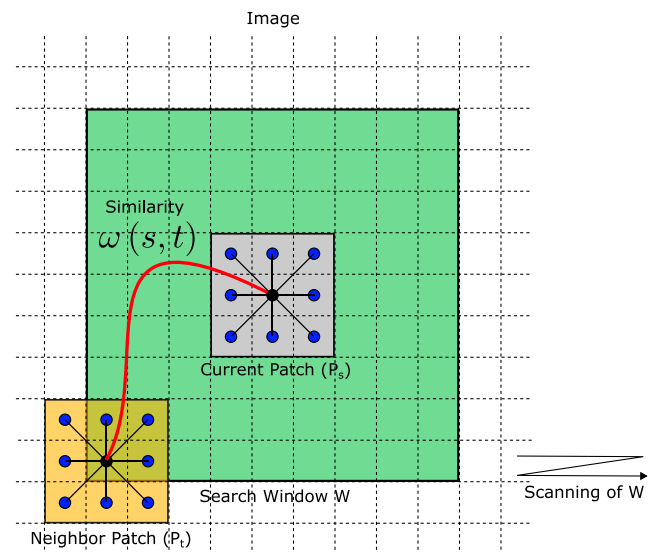
Fig. 2 Illustration of the nonlocal patch-based approach proposed for MRF.
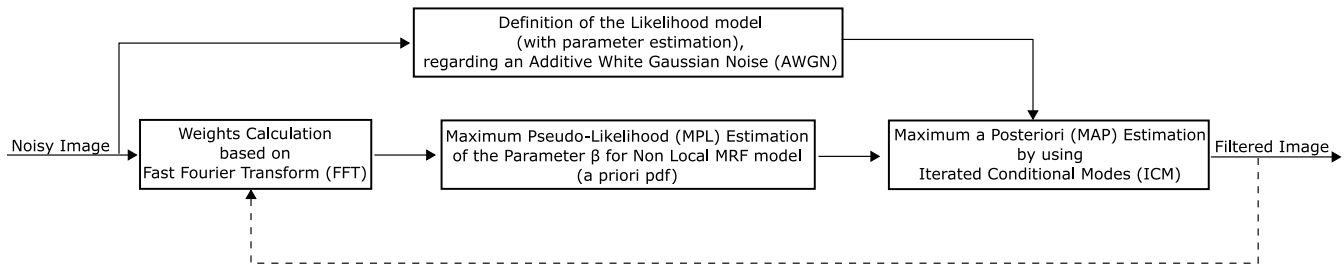
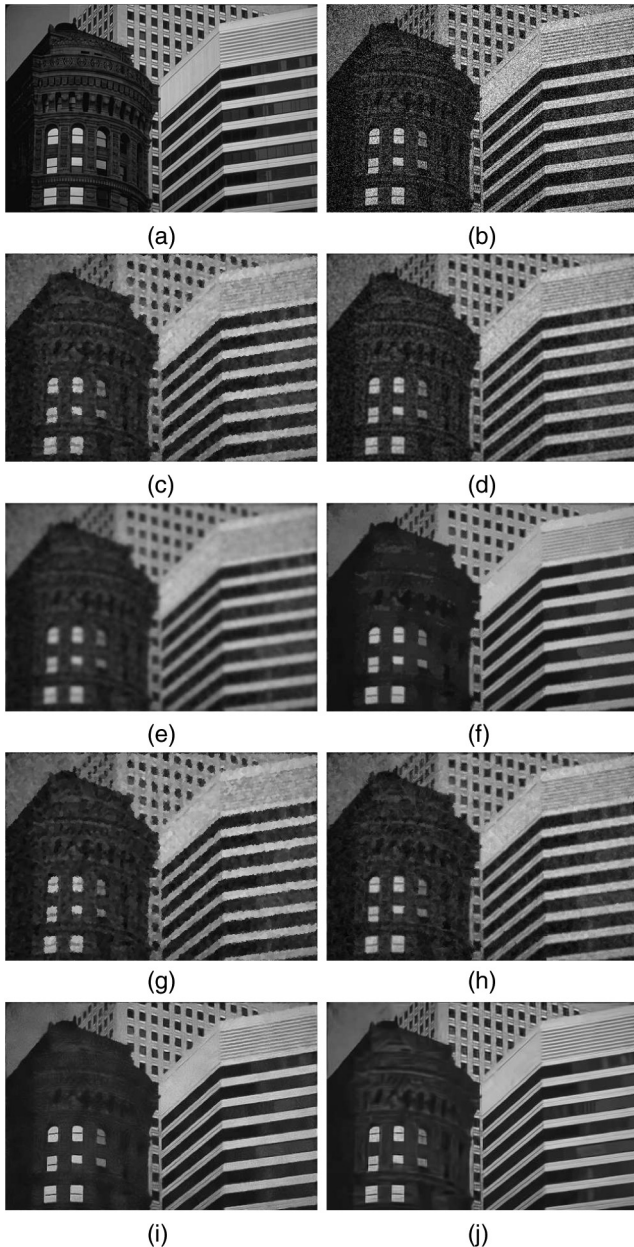**Fig. 3** Block diagram of the proposal methodology, where the dashed line represents an optional step.

Fig. 4 Results for denoising image Buildings by using iterated conditional modes (ICM) and several MRF models, with the noise variance $\sigma^2 = 0.025$: (a) original, (b) noisy, (c) Potts, (d) NLPotts, (e) Gaussian Markov random field (GMRF), (f) nonlocal Gaussian Markov random field (NLGMRF), (g) GIMLL, (h) nonlocal generalized multilevel logistic (NLGIMLL), (i) NLM, and (j) block matching and three-dimensional (BM3D) filtering.
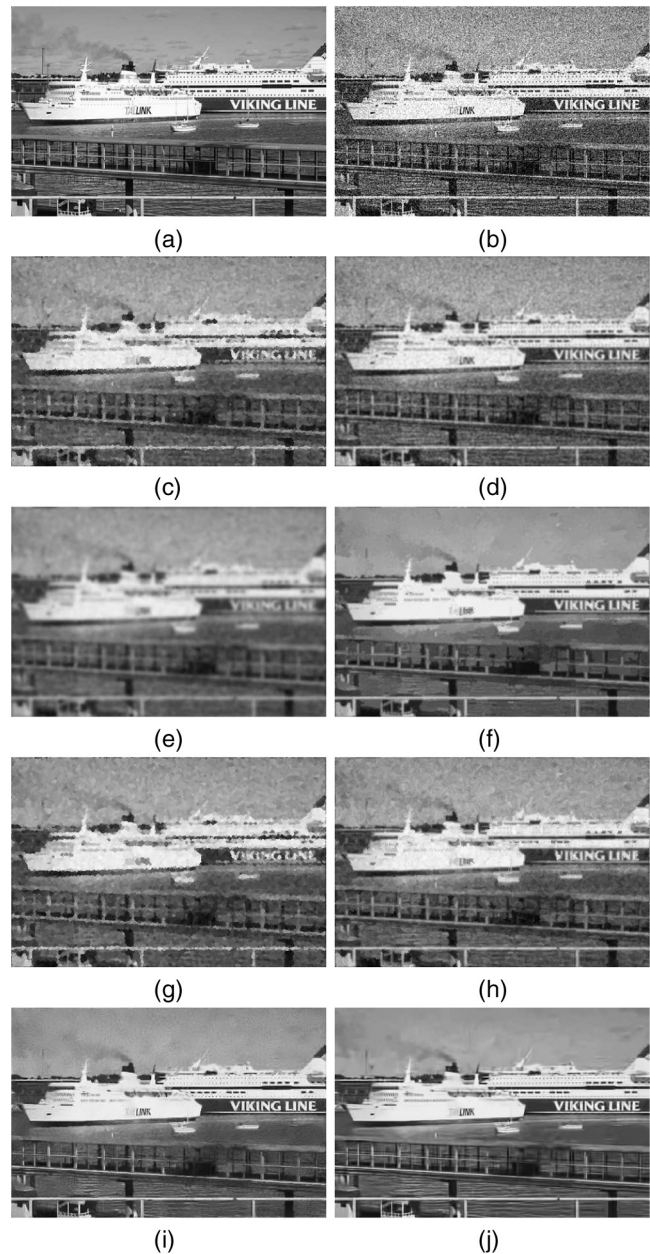
Fig. 5 Results for denoising image Ships by using ICM and several MRF models, with the noise variance $\sigma^2 = 0.025$: (a) original, (b) noisy, (c) Potts, (d) NLPotts, (e) GMRF, (f) NLGMRF, (g) GIMLL, (h) NLGIMLL, (i) NLM, and (j) BM3D.
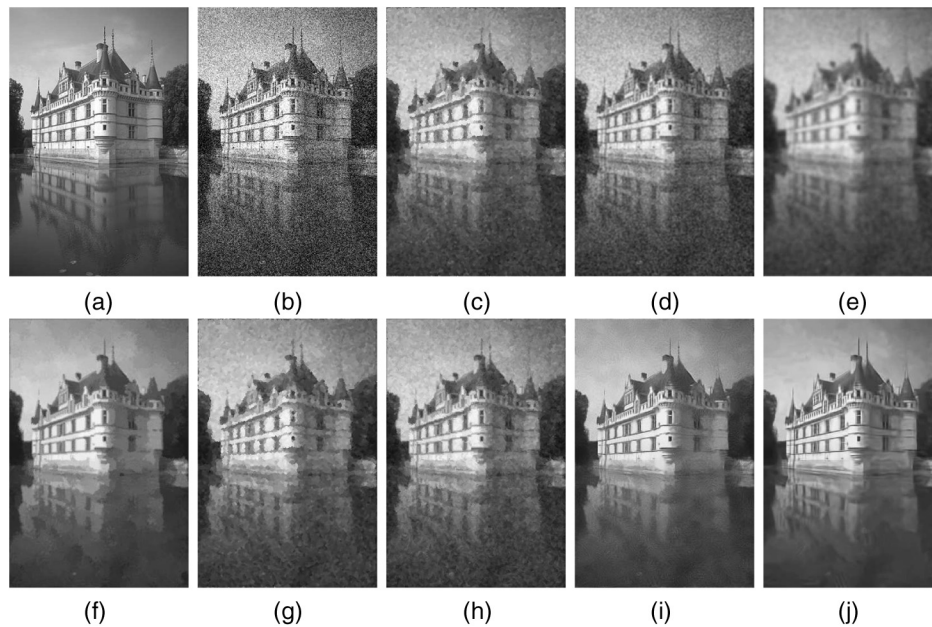
Fig. 6 Results for denoising image Castle by using ICM and several MRF models, with the noise variance $\sigma^2 = 0.025$: (a) original, (b) noisy, (c) Potts, (d) NLPotts, (e) GMRF, (f) NLGMRF, (g) GIMLL, (h) NLGIMLL, (i) NLM, and (j) BM3D.

particle to the total energy depends on the interaction of the particle with its neighbors. In terms of image processing, this means that the definition of a certain pixel depends on its neighborhood only. This defines the Markovianity, that is, the main property of MRF, being described mathematically as[27]

$$p(x_s|\{x_t, t \in L \setminus s\}) = p(x_s|\{x_t, t \in \eta_s\}), \qquad (3)$$

where $L \setminus s$ is the field except the pixel x_s and η_s corresponds to the neighborhood of x_s.

Thus, an MRF defines a local model, which is completely characterized by the local conditional probabilities, given a tuple (L, η), where L is a lattice and η is a neighborhood system.[27]

Besides, an MRF model can be also defined in terms of a Gibbs Markov Random Field (GRF)[27] regarding only the interactions between the current and their neighbor pixels

Fig. 7 Results for denoising image Rope by using ICM and several MRF models, with the noise variance $\sigma^2 = 0.025$: (a) original, (b) noisy, (c) Potts, (d) NLPotts, (e) GMRF, (f) NLGMRF, (g) GIMLL, (h) NLGIMLL, (i) NLM, and (j) BM3D.
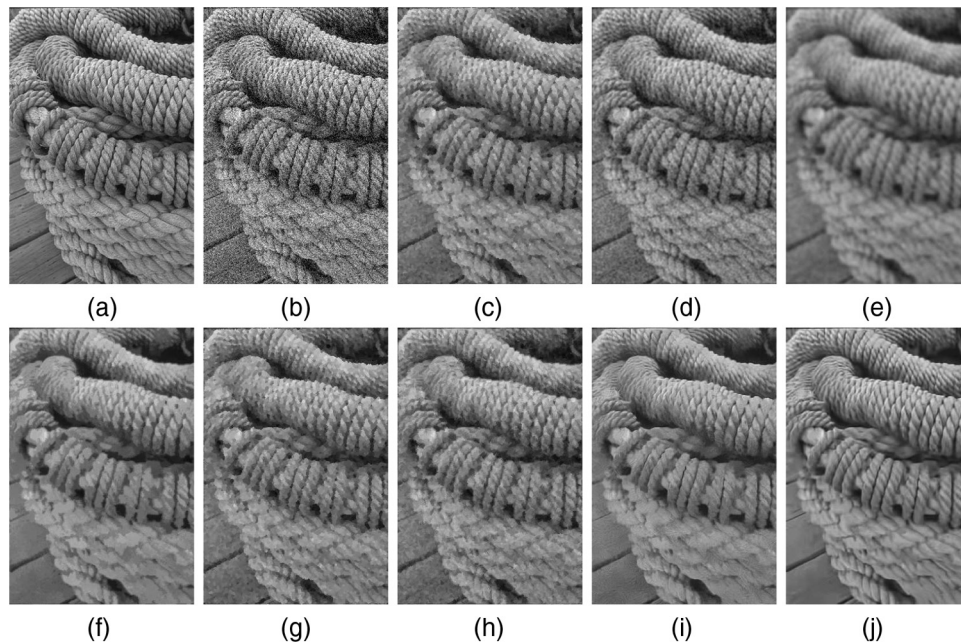
to calculate the global energy from the local energies, as established by the Hammersley–Clifford theorem.[27]

Therefore, an MRF can be globally defined by a Gibbs (joint) distribution:[27]

$$p_x(\vec{x}) = \frac{1}{Z} e^{-U(\vec{x})},\qquad(4)$$

where $U(\vec{x})$ is the energy function and Z is a normalization constant regarding all occurrences of $\vec{x}$.

The energy function $U(\vec{x})$ is calculated as a sum of clique potentials $V_c(\vec{x})$ of all field elements, which is a function of random variables that the field comprises, where $c \in C$ is a clique in the set of all cliques C in a graph G. In graph theory, a clique c is a complete subgraph in a graph G, i.e., all vertices of c have an edge to each other. In images, we can relate a vertex to a pixel and their adjacent vertices to the neighbor pixels.

Mathematically, $U(\vec{x})$ is calculated as a sum of clique potential of all field elements, i.e.,

$$U(\vec{x}) = \sum_{c \in C} V_c(\vec{x}).\qquad(5)$$

In MRF, a clique is conditioned to the chosen neighborhood system. In other words, the global energy is calculated by the influence of the interaction between neighbor pixels of a clique of the pixels in image. However, to calculate the local energy, only the current pixel and its neighbors are considered.

Some local MRF models can be found in the literature.[19,27] First, the Potts model[19] establishes a smoothing constraint in the noise-free pixel estimation, whose local conditional probability is defined by

$$p(x_s = m | \{x_t, t \in \eta_s\}, \beta) = \frac{e^{\beta U_s(m)}}{\sum_l^M e^{\beta U_s(l)}},\qquad(6)$$

where x_s is a pixel at position s, η_s corresponds to the neighborhood of x_s, and m is a pixel value among M possible ones. In our case, M corresponds to the number of levels in the grayscale, i.e., $M = 256$. In turn, $U_s(m)$ is the energy function that corresponds to the number of neighbor pixels that have the same value m and can be described by the following equation:

$$U_s(m) = \sum_{x_t, t \in \eta_s} \delta(m - x_t),\qquad(7)$$

where $\delta(x)$ is a Dirac Delta.

GIMLL[19] extends the Potts model by considering a continuous contribution of the neighbor pixels. Its energy function $U_s(m)$ is defined by

$$U_s(m) = \sum_{x_t, t \in \eta_s} [1 - 2e^{-(m - x_t)^2}].\qquad(8)$$

Finally, another usual model is the GMRF,[19] also called autonormal model, whose local conditional probabilities are given by

$$p(x_s | \{x_t, t \in \eta_s\}, \beta, \mu_s, \sigma_s^2) = \frac{1}{\sqrt{2\pi\sigma_s^2}} e^{\frac{-1}{2\sigma_s^2}[x_s - \mu_s - \beta \sum_{x_t, t \in \eta_s} (x_t - \mu_s)]^2},\qquad(9)$$

where μ_s and σ_s^2 are the local mean and variance estimated in a window around s, respectively.

3 Nonlocal Markov Random Fields

The local MRF models seen in Sec. 2 can be extended to comprise radiometric information by weighting each of the pixelwise interaction pairs according to the similarity
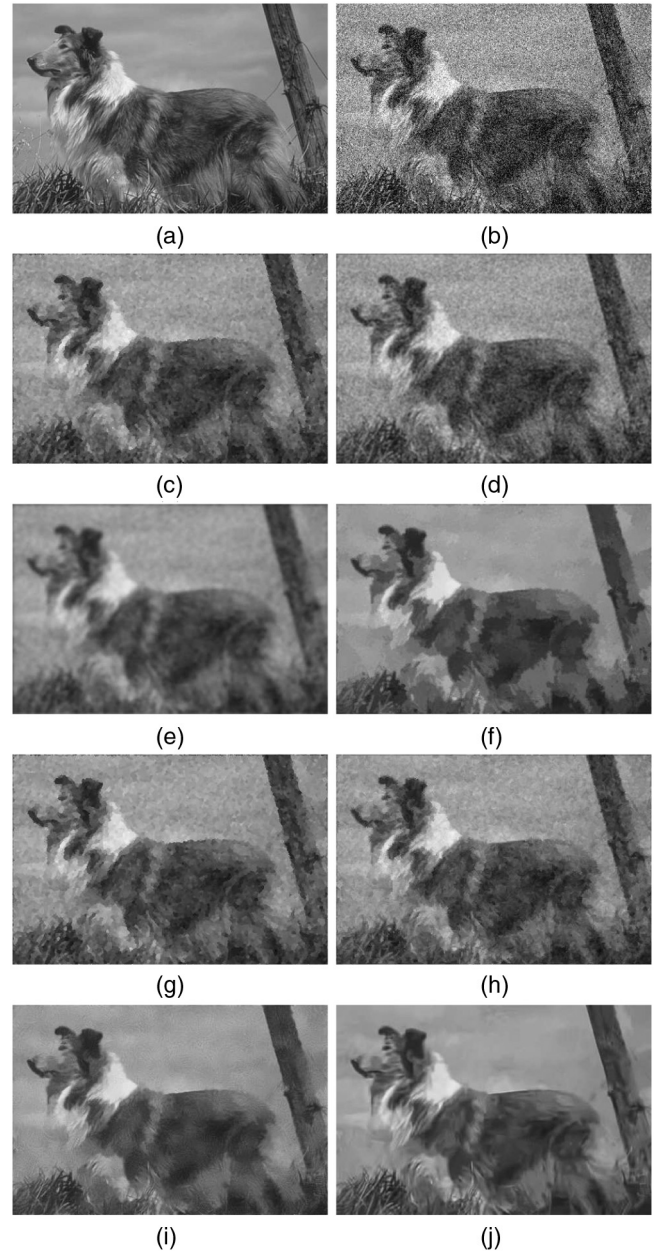
Fig. 8 Results for denoising image Dog by using ICM and several MRF models, with the noise variance $\sigma^2 = 0.025$: (a) original, (b) noisy, (c) Potts, (d) NLPotts, (e) GMRF, (f) NLGMRF, (g) GIMLL, (h) NLGIMLL, (i) NLM, and (j) BM3D.

$\omega(s, t)$ between the current s and their neighbor patches t. This nonlocal patch-based approach is illustrated in Fig. 2. Basically, this modification extends the smoothing constraint to be defined not only in terms of neighbor pixels (local regions) but also by nonlocal regions (patches), which are also restricted to neighbor patches. In other words, there is now a double smoothing constraint, which generates a better model.

The similarities $\omega(s, t)$ can be defined in the same way as done for the NLM method:[4]

$$\omega(s, t) = e^{-\frac{1}{h}\sum_{k \in P} |y_{s,k} - y_{t,k}|^2}, \qquad (10)$$

where k is the k'th pixel in a patch of size P, y is the noisy image, and h controls the smoothing level to be applied. It is important to emphasize that the Euclidean distance is suitable for Gaussian noise. However, similarity measures adapted to other noise distributions (e.g., Gamma, Poisson, or Rayleigh) can be derived as done in Refs. 28–30 by a weighted maximum likelihood estimation (MLE). So, in this case, these new NLMRF models also become adaptive to the kind of noise.

Therefore, based on the proposed idea, nonlocal versions of each model described in Sec. 2 are now described in detail.

Basically, NLPotts and NLGIMLL models can be obtained by changing their local energy functions to incorporate a
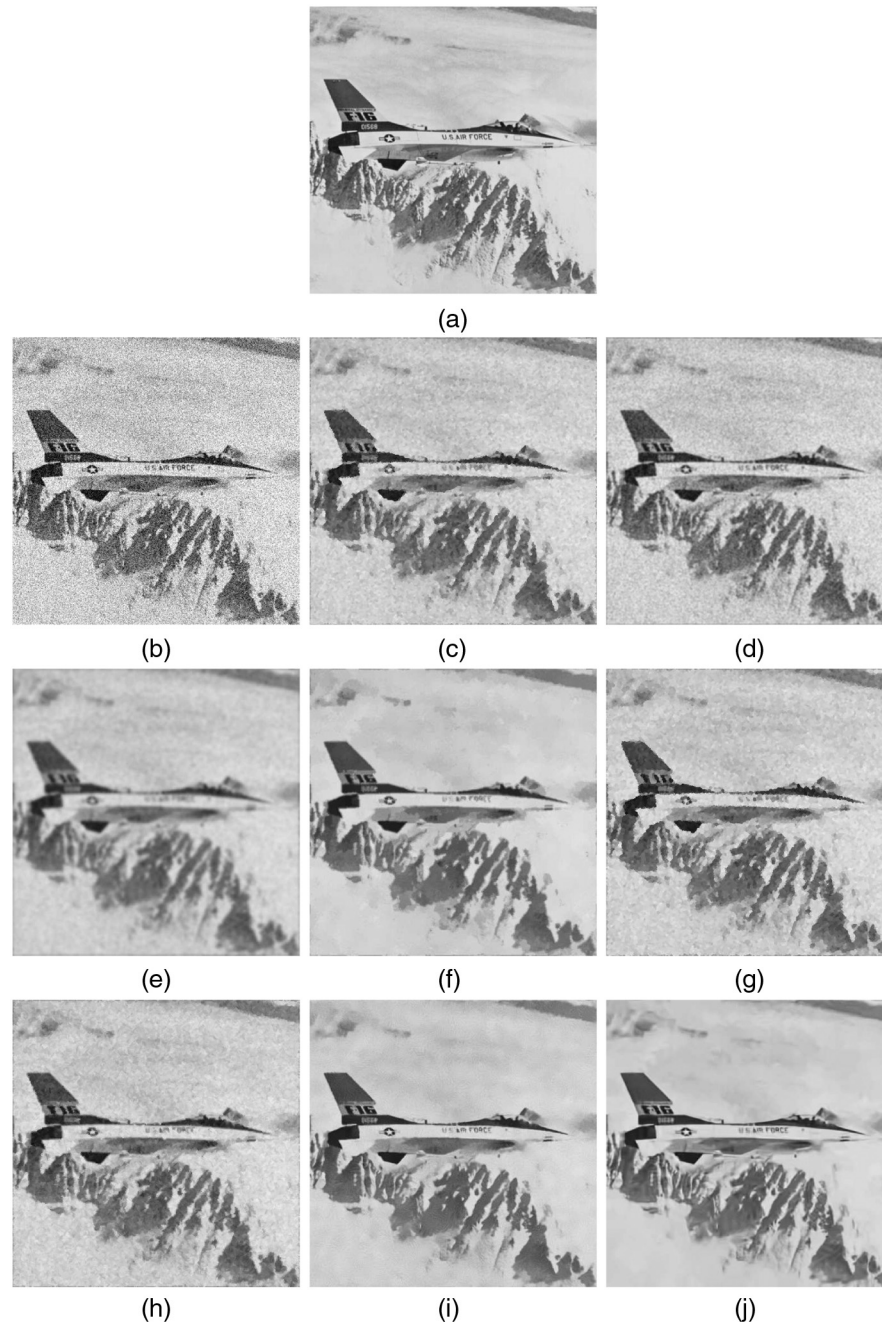
Fig. 9 Results for denoising image Jet Plane by using ICM and several MRF models, with the noise variance $\sigma^2 = 0.025$: (a) original, (b) noisy, (c) Potts, (d) NLPotts, (e) GMRF, (f) NLGMRF, (g) GIMLL, (h) NLGIMLL, (i) NLM, and (j) BM3D.

nonlocal pairwise interaction. Thus, Eqs. (7) and (8) are, respectively, extended to

$$U_s^{\text{NLPotts}}(m) = \sum_{x_t, t \in \eta_s} \omega(s,t)\delta(m - x_t), \qquad (11)$$

$$U_s^{\text{NLGIMLL}}(m) = \sum_{x_t, t \in \eta_s} \omega(s,t)[1 - 2e^{-(m-x_t)^2}]. \qquad (12)$$

In turn, the local conditional probabilities for nonlocal GRMF (NLGMRF) model are defined by

$$p(x_s | \{x_t, t \in \eta_s\}, \beta, \mu_s, \sigma_s^2, \vec{\omega})$$
$$= \frac{1}{\sqrt{2\pi\sigma_s^2}} e^{\frac{-1}{2\sigma_s^2}[x_s - \mu_s - \beta \sum_{x_t, t \in \eta_s} \omega(s,t)(x_t - \mu_s)]^2}, \qquad (13)$$

where $\vec{\omega}$ is a matrix of similarities relating each patch in the image. The factor $\omega(s,t)$ only changes the mean value of x_s. Therefore, the integral of the Gaussian in x_s remains unitary. This means that the pdf in Eq. (13) is a valid probability density function.

It is noteworthy that as the β parameter is a constant, we can define a weighting such that $\beta_{s,t} = \beta\omega(s,t)$. In other

Fig. 10 Results for denoising image Lena by using ICM and several MRF models, with the noise variance $\sigma^2 = 0.025$: (a) original, (b) noisy, (c) Potts, (d) NLPotts, (e) GMRF, (f) NLGMRF, (g) GIMLL, (h) NLGIMLL, (i) NLM, and (j) BM3D.

words, it is equivalent to state that there is a β parameter for each pair of elements s and t in the field. So, these new models seem suitable to represent nonstationary fields.

4 Spatial Dependency Parameter (β) Estimation

The common parameter for all cited MRF models in this paper is the spatial dependency parameter β. This parameter is defined as the inverse temperature of the system at that particular moment (the higher the temperature, the lower the strength of interactions). In other words, it is necessary to know β to infer some thermodynamic properties of the system (statistics, information-theoretic measures, etc.)

when it is operating under a given regime. Although we are dealing with a static 2-D image, as a snapshot of the system, it is necessary to know the approximate temperature of the system at the time this picture was taken, which is a key aspect to compute the intrinsic properties of the system at that particular moment. The inverse temperature parameter provides valuable information about the expected global behavior. So, the definition of the parameter β is essential for a suitable modeling of the constraint.

Due to the intractability of the parameter Z of GRF, estimating parameters of this distribution by using an MLE is impracticable. In general, an MPLE, proposed by Ref. 31,

Fig. 11 Results for denoising image House by using ICM and several MRF models, with the noise variance $\sigma^2 = 0.025$: (a) original, (b) noisy, (c) Potts, (d) NLPotts, (e) GMRF, (f) NLGMRF, (g) GIMLL, (h) NLGIMLL, (i) NLM, and (j) BM3D.
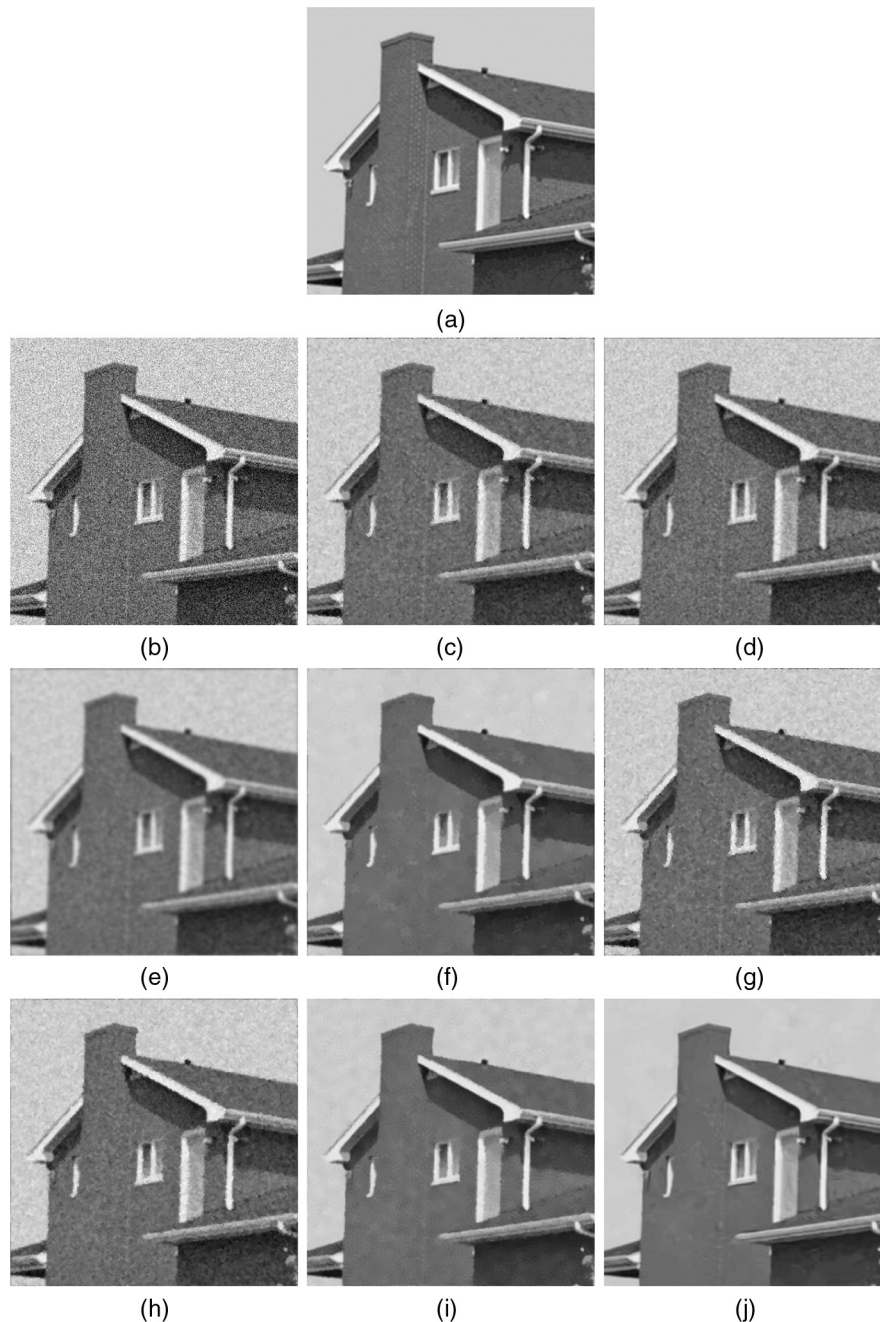
is used, whose method uses the local conditional probabilities instead of the joint distribution.

In the literature, the MPLE estimation for Potts,[32] GIMLL,[33] and GMRF[19] can be found. Therefore, in this section, the MPLE of this parameter for each new proposed nonlocal MRF models is defined.

To obtain an MPLE estimation for these Potts-based models, the following equation can be numerically solved:

$$\sum_s^N U_s(m) - \sum_s^N \frac{\sum_l^M U_s(l)e^{\beta U_s(l)}}{\sum_l^M e^{\beta U_s(l)}}, \qquad (14)$$

where N is the number of pixels in the image and $U_s(m)$ is the energy function that can be defined according to Eqs. (11) and (12) for NLPotts and NLGIMLL, respectively.

Finally, the MPLE estimation of the β parameter of the NLGMRF can be defined in a closed formula:

$$\hat{\beta}_{\text{MPLE}} = \frac{\sum_s [(x_s - \mu) \sum_{x_t, t \in \eta_s} \omega(s,t)(x_t - \mu)]}{\sum_s [\sum_{x_t, t \in \eta_s} \omega(s,t)(x_t - \mu)]^2}, \qquad (15)$$

where μ is the global mean of the observed image.
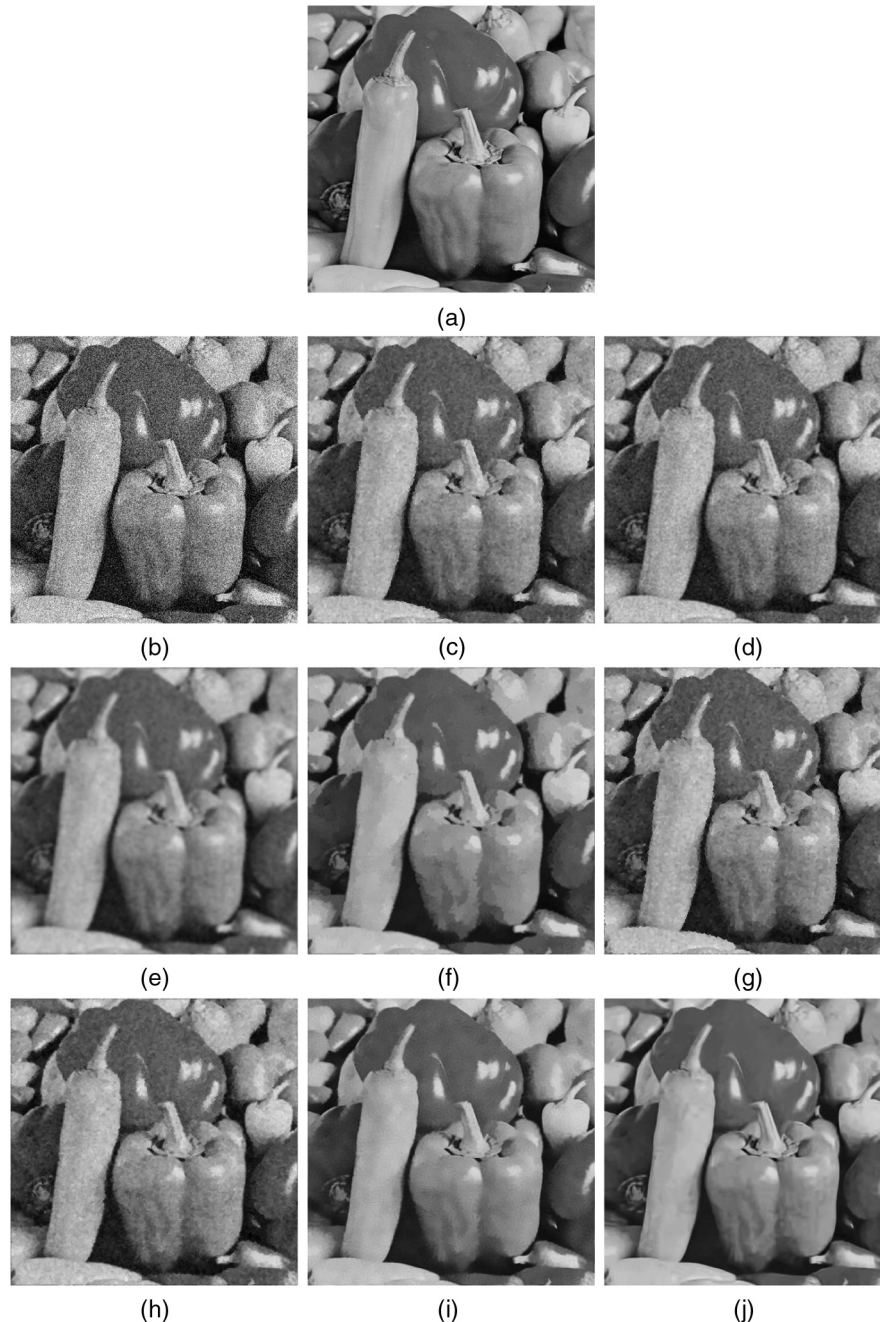
Fig. 12 Results for denoising image Peppers by using ICM and several MRF models, with the noise variance $\sigma^2 = 0.025$: (a) original, (b) noisy, (c) Potts, (d) NLPotts, (e) GMRF, (f) NLGMRF, (g) GIMLL, (h) NLGIMLL, (i) NLM, and (j) BM3D.

5 Evaluation Setup

Basically, to evaluate the new NLMRF priors proposed in this paper, an MAP–MRF framework was used to denoise images corrupted by additive white Gaussian noise (AWGN). Thus, the likelihood was modeled by a Gaussian distribution.

Moreover, to obtain an approximate MAP estimation, the classical iterated conditional modes (ICM) algorithm[34] was used, running seven iterations at most. The complexity time for ICM with classical MRF models is $\mathcal{O}(|N|)$ for each iteration, where $|N|$ is the number of pixels in an image.

In addition, Brent's method[35] was chosen to obtain the numerical solutions of the MPLE of the parameter β for NLPotts and NLGIMLL, as well as for their local version. In the case of NLGMRF and GMRF, there is a closed formula to estimate this parameter; therefore, a direct solution was obtained.

Also, to determine the weights $\omega(s, t)$, the algorithm proposed in Ref. 36 was used, which calculates the weights for the NLM by a fast Fourier transform. It is important to emphasize that only the part of weights calculation from this algorithm was used here and not the whole NLM algorithm.

Fig. 13 Results for denoising image Walk Bridge by using ICM and several MRF models, with the noise variance $\sigma^2 = 0.025$: (a) original, (b) noisy, (c) Potts, (d) NLPotts, (e) GMRF, (f) NLGMRF, (g) GIMLL, (h) NLGIMLL, (i) NLM, and (j) BM3D.
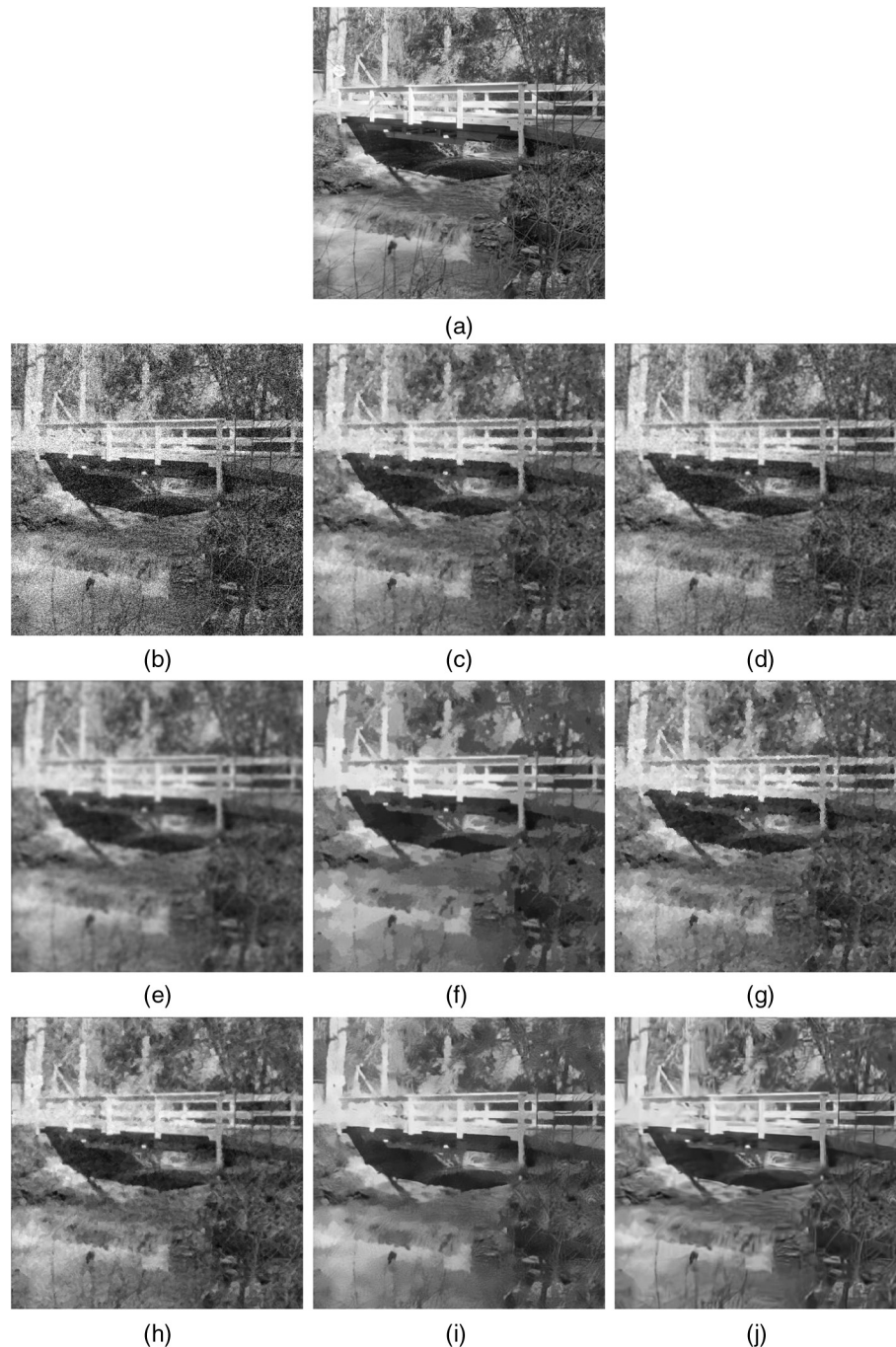
Table 1 Denoising results in terms of peak signal-to-noise ratio (PSNR) for noise variance $\sigma^2 = 0.010$.

Images	Noisy	Potts	NLPotts	GMRF	NLGMRF	GIMLL	NLGIMLL	NLM	BM3D	Mean (Std)
Swan	20.64 (0.02)	25.16 (0.06)	26.96 (0.01)	24.78 (0.01)	26.64 (0.03)	25.00 (0.09)	25.95 (0.04)	29.40 (0.04)	31.18 (0.03)	26.59 (2.03)
Sea Star	20.21 (0.01)	23.38 (0.04)	25.92 (0.01)	22.99 (0.01)	24.35 (0.03)	23.01 (0.03)	23.93 (0.04)	26.12 (0.03)	28.26 (0.02)	24.47 (1.69)
Eskimo	20.23 (0.01)	24.80 (0.05)	26.76 (0.02)	24.75 (0.01)	25.38 (0.03)	24.49 (0.06)	25.14 (0.03)	26.77 (0.03)	28.39 (0.03)	25.60 (1.24)
Bridge	20.59 (0.01)	22.56 (0.07)	24.41 (0.01)	22.10 (0.01)	23.77 (0.03)	22.22 (0.07)	23.36 (0.02)	26.18 (0.02)	28.18 (0.03)	23.82 (1.90)
Butterfly	20.18 (0.02)	22.46 (0.05)	24.99 (0.01)	21.87 (0.01)	23.88 (0.03)	22.18 (0.07)	23.17 (0.02)	26.75 (0.03)	28.82 (0.03)	23.92 (2.19)
Buildings	20.60 (0.02)	21.14 (0.04)	23.11 (0.02)	20.12 (0.01)	22.74 (0.02)	20.86 (0.07)	22.40 (0.01)	26.45 (0.03)	29.50 (0.04)	22.94 (2.78)
Boat and Bridge	20.26 (0.02)	24.10 (0.04)	25.42 (0.01)	23.79 (0.01)	24.79 (0.03)	23.83 (0.03)	24.59 (0.03)	26.82 (0.03)	28.76 (0.03)	25.04 (1.53)
Ostrich	20.12 (0.02)	27.59 (0.03)	28.69 (0.02)	28.29 (0.02)	28.66 (0.03)	27.51 (0.03)	27.48 (0.05)	29.74 (0.02)	30.99 (0.04)	28.39 (1.14)
Ships	20.36 (0.02)	18.92 (0.04)	20.64 (0.01)	18.03 (0.00)	20.13 (0.01)	18.52 (0.03)	19.85 (0.02)	24.01 (0.02)	27.10 (0.04)	20.54 (2.73)
Buildings and Boats	20.44 (0.01)	19.30 (0.05)	20.89 (0.01)	18.60 (0.00)	20.01 (0.01)	18.98 (0.05)	19.87 (0.01)	22.88 (0.01)	25.50 (0.03)	20.47 (2.06)
Castle	20.14 (0.01)	23.28 (0.05)	24.70 (0.01)	22.87 (0.01)	24.22 (0.01)	23.04 (0.04)	23.77 (0.02)	27.04 (0.04)	29.31 (0.04)	24.49 (2.00)
Horses	20.16 (0.02)	22.19 (0.04)	23.36 (0.01)	21.83 (0.01)	22.27 (0.02)	21.94 (0.03)	22.14 (0.03)	23.79 (0.02)	26.10 (0.02)	22.76 (1.29)
Miscellaneous	20.24 (0.01)	21.12 (0.04)	22.56 (0.01)	20.35 (0.01)	21.85 (0.03)	20.81 (0.05)	21.55 (0.02)	24.54 (0.03)	27.26 (0.04)	22.23 (2.04)
Rope	20.07 (0.02)	22.13 (0.02)	23.96 (0.01)	21.25 (0.01)	22.46 (0.02)	21.75 (0.04)	22.22 (0.03)	23.87 (0.02)	26.15 (0.01)	22.76 (1.42)
Corn	20.24 (0.01)	21.65 (0.03)	24.47 (0.01)	20.87 (0.01)	22.33 (0.03)	21.15 (0.05)	21.75 (0.06)	24.46 (0.02)	27.54 (0.02)	22.68 (2.06)
Dog	20.06 (0.02)	25.27 (0.04)	26.78 (0.02)	25.23 (0.01)	25.69 (0.03)	25.07 (0.05)	25.38 (0.03)	27.15 (0.03)	28.99 (0.04)	25.99 (1.22)
Zebra	20.09 (0.01)	20.43 (0.04)	21.81 (0.01)	19.26 (0.00)	21.24 (0.02)	20.16 (0.06)	20.72 (0.02)	25.42 (0.03)	27.40 (0.03)	21.71 (2.49)
Church	20.09 (0.01)	20.88 (0.02)	22.32 (0.00)	20.03 (0.00)	21.82 (0.01)	20.54 (0.02)	21.62 (0.02)	24.48 (0.03)	27.59 (0.04)	22.13 (2.19)
Taj Mahal	20.28 (0.02)	22.52 (0.04)	24.36 (0.01)	21.73 (0.01)	23.77 (0.02)	22.16 (0.03)	23.34 (0.03)	26.80 (0.03)	28.94 (0.03)	23.89 (2.20)
Woman	20.11 (0.01)	24.40 (0.05)	26.66 (0.02)	23.71 (0.02)	25.47 (0.03)	23.75 (0.07)	24.64 (0.04)	27.26 (0.03)	30.48 (0.04)	25.43 (2.09)
Jet Plane	20.18 (0.01)	25.15 (0.04)	27.65 (0.01)	24.88 (0.01)	26.91 (0.03)	24.87 (0.05)	25.87 (0.05)	29.41 (0.04)	31.56 (0.03)	26.68 (2.17)
Lake	20.18 (0.01)	23.84 (0.02)	26.67 (0.02)	23.52 (0.00)	25.01 (0.02)	23.48 (0.05)	24.26 (0.03)	27.00 (0.02)	29.11 (0.02)	25.04 (1.84)
Living Room	20.10 (0.01)	24.39 (0.03)	26.24 (0.01)	23.91 (0.01)	25.28 (0.02)	24.03 (0.03)	24.87 (0.03)	26.78 (0.02)	29.51 (0.02)	25.37 (1.67)
Pirate	20.08 (0.01)	25.36 (0.02)	27.20 (0.01)	25.04 (0.01)	26.13 (0.03)	25.04 (0.03)	25.61 (0.03)	27.57 (0.02)	29.47 (0.02)	26.19 (1.40)
Cameraman	20.39 (0.01)	25.48 (0.05)	28.18 (0.02)	25.13 (0.01)	28.01 (0.04)	25.24 (0.05)	26.62 (0.05)	30.19 (0.04)	32.43 (0.04)	27.30 (2.34)
Lena	20.07 (0.01)	26.31 (0.06)	28.49 (0.03)	26.37 (0.01)	28.02 (0.04)	26.05 (0.06)	26.90 (0.05)	29.91 (0.04)	31.97 (0.06)	27.68 (1.88)
House	20.13 (0.01)	27.07 (0.07)	29.88 (0.02)	28.28 (0.02)	30.97 (0.04)	26.97 (0.06)	28.68 (0.03)	33.36 (0.04)	35.46 (0.05)	29.62 (2.75)
Mandril	20.03 (0.01)	23.30 (0.02)	25.38 (0.01)	22.38 (0.01)	23.24 (0.03)	22.80 (0.02)	23.10 (0.01)	24.83 (0.02)	27.72 (0.02)	23.85 (1.59)
Peppers	20.17 (0.01)	26.08 (0.04)	28.23 (0.02)	26.58 (0.02)	28.01 (0.05)	25.91 (0.08)	26.82 (0.05)	29.92 (0.03)	31.21 (0.02)	27.53 (1.74)
Walk Bridge	20.16 (0.01)	22.70 (0.01)	24.52 (0.01)	22.09 (0.01)	22.99 (0.02)	22.29 (0.02)	22.92 (0.01)	24.32 (0.01)	26.34 (0.01)	23.32 (1.29)
Mean	20.22 (0.16)	23.43 (2.17)	25.37 (2.34)	23.02 (2.60)	24.53 (2.58)	23.12 (2.22)	23.95 (2.21)	26.77 (2.36)	29.04 (2.15)	24.61 (2.97)

Note: GMRF, Gaussian Markov random field; NLGMRF, nonlocal Gaussian Markov random field; GIMLL, generalized multilevel logistic; NLGIMLL, nonlocal generalized multi-level logistic; NLM, nonlocal means; BM3D, block matching and three-dimensional filtering.

Table 2 Denoising results in terms of structural similarity index (SSIM) for noise variance $\sigma^2 = 0.010$.

| Images	Noisy	Potts	NLPotts	GMRF	NLGMRF	GIMLL	NLGIMLL	NLM	BM3D	Mean (Std)
Swan	0.27 (0.00)	0.68 (0.00)	0.72 (0.00)	0.71 (0.00)	0.73 (0.00)	0.68 (0.00)	0.66 (0.00)	0.77 (0.00)	0.83 (0.00)	0.71 (0.05)
Sea Star	0.41 (0.00)	0.63 (0.00)	0.74 (0.00)	0.61 (0.00)	0.66 (0.00)	0.61 (0.00)	0.63 (0.00)	0.72 (0.00)	0.80 (0.00)	0.66 (0.07)
Eskimo	0.36 (0.00)	0.60 (0.00)	0.69 (0.00)	0.58 (0.00)	0.59 (0.00)	0.58 (0.00)	0.58 (0.00)	0.65 (0.00)	0.74 (0.00)	0.62 (0.05)
Bridge	0.38 (0.00)	0.59 (0.00)	0.64 (0.00)	0.56 (0.00)	0.63 (0.00)	0.58 (0.00)	0.59 (0.00)	0.70 (0.00)	0.78 (0.00)	0.62 (0.07)
Butterfly	0.42 (0.00)	0.66 (0.00)	0.75 (0.00)	0.65 (0.00)	0.72 (0.00)	0.65 (0.00)	0.66 (0.00)	0.79 (0.00)	0.85 (0.00)	0.70 (0.07)
Buildings	0.50 (0.00)	0.58 (0.00)	0.65 (0.00)	0.48 (0.00)	0.62 (0.00)	0.57 (0.00)	0.60 (0.00)	0.74 (0.00)	0.85 (0.00)	0.63 (0.10)
Boat and Bridge	0.34 (0.00)	0.56 (0.00)	0.62 (0.00)	0.54 (0.00)	0.57 (0.00)	0.55 (0.00)	0.55 (0.00)	0.66 (0.00)	0.75 (0.00)	0.59 (0.06)
Ostrich	0.21 (0.00)	0.69 (0.00)	0.69 (0.00)	0.80 (0.00)	0.82 (0.00)	0.71 (0.00)	0.66 (0.00)	0.83 (0.00)	0.87 (0.00)	0.74 (0.07)
Ships	0.53 (0.00)	0.53 (0.00)	0.61 (0.00)	0.46 (0.00)	0.60 (0.00)	0.51 (0.00)	0.56 (0.00)	0.76 (0.00)	0.87 (0.00)	0.60 (0.12)
Buildings and Boats	0.58 (0.00)	0.49 (0.00)	0.58 (0.00)	0.41 (0.00)	0.51 (0.00)	0.46 (0.00)	0.50 (0.00)	0.66 (0.00)	0.79 (0.00)	0.54 (0.11)
Castle	0.30 (0.00)	0.63 (0.00)	0.67 (0.00)	0.68 (0.00)	0.73 (0.00)	0.64 (0.00)	0.62 (0.00)	0.78 (0.00)	0.85 (0.00)	0.69 (0.07)
Horses	0.44 (0.00)	0.53 (0.00)	0.62 (0.00)	0.47 (0.00)	0.49 (0.00)	0.50 (0.00)	0.50 (0.00)	0.59 (0.00)	0.73 (0.00)	0.54 (0.08)
Miscellaneous	0.40 (0.00)	0.59 (0.00)	0.63 (0.00)	0.58 (0.00)	0.66 (0.00)	0.59 (0.00)	0.58 (0.00)	0.75 (0.00)	0.83 (0.00)	0.64 (0.08)
Rope	0.54 (0.00)	0.55 (0.00)	0.66 (0.00)	0.42 (0.00)	0.53 (0.00)	0.52 (0.00)	0.53 (0.00)	0.63 (0.00)	0.76 (0.00)	0.56 (0.09)
Corn	0.53 (0.00)	0.62 (0.00)	0.75 (0.00)	0.54 (0.00)	0.64 (0.00)	0.58 (0.00)	0.60 (0.00)	0.73 (0.00)	0.85 (0.00)	0.65 (0.09)
Dog	0.32 (0.00)	0.61 (0.00)	0.67 (0.00)	0.62 (0.00)	0.65 (0.00)	0.60 (0.00)	0.59 (0.00)	0.71 (0.00)	0.79 (0.00)	0.64 (0.06)
Zebra	0.41 (0.00)	0.57 (0.00)	0.65 (0.00)	0.54 (0.00)	0.60 (0.00)	0.56 (0.00)	0.55 (0.00)	0.71 (0.00)	0.78 (0.00)	0.61 (0.08)
Church	0.54 (0.00)	0.51 (0.00)	0.60 (0.00)	0.41 (0.00)	0.57 (0.00)	0.49 (0.00)	0.54 (0.00)	0.72 (0.00)	0.86 (0.00)	0.57 (0.12)
Taj Mahal	0.35 (0.00)	0.64 (0.00)	0.68 (0.00)	0.66 (0.00)	0.74 (0.00)	0.64 (0.00)	0.64 (0.00)	0.81 (0.00)	0.86 (0.00)	0.69 (0.08)
Woman	0.32 (0.00)	0.66 (0.00)	0.72 (0.00)	0.66 (0.00)	0.73 (0.00)	0.65 (0.00)	0.64 (0.00)	0.77 (0.00)	0.85 (0.00)	0.70 (0.07)
Jet Plane	0.28 (0.00)	0.70 (0.00)	0.75 (0.00)	0.76 (0.00)	0.80 (0.00)	0.71 (0.00)	0.69 (0.00)	0.84 (0.00)	0.88 (0.00)	0.75 (0.07)
Lake	0.36 (0.00)	0.64 (0.00)	0.72 (0.00)	0.65 (0.00)	0.70 (0.00)	0.64 (0.00)	0.63 (0.00)	0.75 (0.00)	0.81 (0.00)	0.68 (0.06)
Living Room	0.36 (0.00)	0.61 (0.00)	0.69 (0.00)	0.58 (0.00)	0.64 (0.00)	0.59 (0.00)	0.60 (0.00)	0.70 (0.00)	0.81 (0.00)	0.64 (0.07)
Pirate	0.32 (0.00)	0.64 (0.00)	0.71 (0.00)	0.64 (0.00)	0.68 (0.00)	0.63 (0.00)	0.62 (0.00)	0.72 (0.00)	0.80 (0.00)	0.67 (0.06)
Cameraman	0.26 (0.00)	0.71 (0.00)	0.75 (0.00)	0.77 (0.00)	0.82 (0.00)	0.72 (0.00)	0.70 (0.00)	0.83 (0.00)	0.89 (0.00)	0.76 (0.06)
Lena	0.26 (0.00)	0.68 (0.00)	0.73 (0.00)	0.75 (0.00)	0.78 (0.00)	0.69 (0.00)	0.67 (0.00)	0.81 (0.00)	0.86 (0.00)	0.73 (0.06)
House	0.20 (0.00)	0.74 (0.00)	0.77 (0.00)	0.84 (0.00)	0.87 (0.00)	0.75 (0.00)	0.73 (0.00)	0.87 (0.00)	0.92 (0.00)	0.80 (0.07)
Mandril	0.46 (0.00)	0.59 (0.00)	0.72 (0.00)	0.46 (0.00)	0.54 (0.00)	0.54 (0.00)	0.55 (0.00)	0.65 (0.00)	0.81 (0.00)	0.59 (0.10)
Peppers	0.27 (0.00)	0.65 (0.00)	0.70 (0.00)	0.72 (0.00)	0.73 (0.00)	0.66 (0.00)	0.64 (0.00)	0.77 (0.00)	0.79 (0.00)	0.69 (0.05)
Walk Bridge	0.49 (0.00)	0.55 (0.00)	0.66 (0.00)	0.46 (0.00)	0.51 (0.00)	0.51 (0.00)	0.53 (0.00)	0.60 (0.00)	0.74 (0.00)	0.56 (0.08)
Mean	0.38 (0.10)	0.61 (0.06)	0.68 (0.05)	0.60 (0.12)	0.66 (0.10)	0.60 (0.07)	0.61 (0.06)	0.73 (0.07)	0.82 (0.05)	0.65 (0.10)

Table 3 Denoising results in terms of PSNR for noise variance $\sigma^2 = 0.025$.

Images	Noisy	Potts	NLPotts	GMRF	NLGMRF	GIMLL	NLGIMLL	NLM	BM3D	Mean (Std)
Swan	17.19 (0.01)	24.05 (0.04)	25.24 (0.02)	24.04 (0.02)	25.95 (0.03)	24.02 (0.06)	24.60 (0.05)	27.35 (0.05)	28.30 (0.05)	25.22 (1.46)
Sea Star	16.48 (0.02)	22.67 (0.04)	24.66 (0.04)	22.68 (0.02)	23.46 (0.02)	22.48 (0.04)	22.79 (0.03)	24.85 (0.03)	25.89 (0.04)	23.46 (1.17)
Eskimo	16.42 (0.02)	23.81 (0.03)	25.24 (0.02)	24.31 (0.02)	24.58 (0.03)	23.71 (0.05)	23.86 (0.03)	25.53 (0.03)	26.50 (0.03)	24.50 (0.92)
Bridge	16.89 (0.02)	21.83 (0.05)	23.27 (0.02)	21.63 (0.01)	23.12 (0.03)	21.65 (0.04)	22.39 (0.04)	24.79 (0.04)	25.55 (0.03)	22.81 (1.33)
Butterfly	16.56 (0.01)	21.87 (0.02)	23.95 (0.03)	21.60 (0.02)	23.14 (0.04)	21.70 (0.03)	22.24 (0.04)	25.23 (0.04)	26.06 (0.03)	22.96 (1.54)
Buildings	17.02 (0.03)	20.57 (0.05)	22.24 (0.02)	19.79 (0.01)	22.20 (0.03)	20.38 (0.04)	21.56 (0.03)	24.88 (0.04)	26.14 (0.05)	21.96 (1.97)
Boat and Bridge	16.49 (0.01)	23.25 (0.03)	24.25 (0.02)	23.43 (0.01)	24.32 (0.03)	23.16 (0.03)	23.50 (0.03)	25.65 (0.04)	26.58 (0.05)	24.07 (1.12)
Ostrich	16.44 (0.02)	26.11 (0.03)	26.79 (0.04)	27.71 (0.03)	27.66 (0.05)	26.24 (0.05)	25.85 (0.03)	27.95 (0.04)	29.36 (0.04)	26.98 (1.10)
Ships	16.59 (0.01)	18.61 (0.02)	20.11 (0.01)	17.87 (0.01)	19.74 (0.02)	18.35 (0.04)	19.35 (0.02)	22.86 (0.04)	23.90 (0.03)	19.83 (1.92)
Buildings and Boats	16.77 (0.01)	18.99 (0.03)	20.36 (0.01)	18.41 (0.00)	19.60 (0.02)	18.77 (0.04)	19.37 (0.02)	22.00 (0.02)	22.69 (0.02)	19.82 (1.38)
Castle	16.41 (0.02)	22.63 (0.03)	23.75 (0.02)	22.64 (0.01)	23.66 (0.05)	22.55 (0.03)	22.88 (0.03)	25.64 (0.05)	26.78 (0.04)	23.59 (1.41)
Horses	16.42 (0.01)	21.66 (0.02)	22.61 (0.01)	21.64 (0.01)	21.93 (0.03)	21.50 (0.03)	21.51 (0.03)	23.28 (0.03)	23.69 (0.04)	22.07 (0.79)
Miscellaneous	16.55 (0.02)	20.67 (0.03)	21.89 (0.02)	20.16 (0.01)	21.47 (0.03)	20.48 (0.03)	20.99 (0.03)	23.61 (0.03)	24.48 (0.04)	21.51 (1.38)
Rope	16.26 (0.02)	21.56 (0.02)	23.13 (0.02)	21.09 (0.01)	21.78 (0.03)	21.32 (0.03)	21.35 (0.03)	23.10 (0.03)	24.16 (0.03)	22.00 (1.01)
Corn	16.62 (0.02)	21.19 (0.03)	23.51 (0.03)	20.65 (0.01)	21.67 (0.03)	20.84 (0.04)	21.03 (0.04)	23.43 (0.02)	24.85 (0.03)	21.88 (1.43)
Dog	16.27 (0.02)	24.27 (0.03)	25.38 (0.03)	24.92 (0.02)	24.95 (0.03)	24.22 (0.05)	24.13 (0.05)	25.96 (0.03)	26.99 (0.02)	24.91 (0.92)
Zebra	16.24 (0.01)	20.04 (0.04)	21.23 (0.01)	19.15 (0.00)	20.86 (0.03)	19.84 (0.03)	20.27 (0.01)	24.25 (0.02)	24.85 (0.03)	21.05 (1.85)
Church	16.33 (0.02)	20.48 (0.01)	21.74 (0.01)	19.92 (0.01)	21.25 (0.02)	20.25 (0.02)	20.79 (0.02)	23.41 (0.03)	24.92 (0.04)	21.37 (1.53)
Taj Mahal	16.53 (0.01)	21.92 (0.02)	23.38 (0.02)	21.47 (0.01)	23.20 (0.03)	21.72 (0.04)	22.41 (0.03)	25.23 (0.05)	26.22 (0.04)	22.95 (1.54)
Woman	16.32 (0.02)	23.53 (0.06)	25.21 (0.02)	23.43 (0.02)	24.60 (0.05)	23.22 (0.05)	23.49 (0.06)	25.74 (0.04)	27.74 (0.03)	24.34 (1.44)
Jet Plane	16.65 (0.01)	24.21 (0.04)	26.03 (0.03)	24.48 (0.02)	26.11 (0.04)	24.07 (0.04)	24.50 (0.05)	27.48 (0.03)	29.13 (0.05)	25.45 (1.65)
Lake	16.58 (0.01)	23.14 (0.04)	25.30 (0.02)	23.20 (0.02)	24.23 (0.05)	22.94 (0.03)	23.19 (0.05)	25.68 (0.03)	26.92 (0.03)	24.05 (1.36)
Living Room	16.27 (0.02)	23.52 (0.02)	24.91 (0.02)	23.62 (0.01)	24.40 (0.02)	23.33 (0.03)	23.51 (0.04)	25.47 (0.03)	27.13 (0.03)	24.26 (1.20)
Pirate	16.32 (0.01)	24.33 (0.03)	25.70 (0.02)	24.73 (0.02)	25.28 (0.03)	24.20 (0.04)	24.22 (0.03)	26.22 (0.02)	27.48 (0.02)	25.05 (1.07)
Cameraman	16.58 (0.01)	24.25 (0.03)	25.97 (0.03)	24.42 (0.02)	26.92 (0.04)	24.18 (0.06)	24.80 (0.05)	27.53 (0.05)	29.43 (0.08)	25.64 (1.71)
Lena	16.28 (0.01)	25.06 (0.03)	26.55 (0.02)	25.93 (0.01)	26.84 (0.03)	25.03 (0.03)	25.12 (0.02)	27.67 (0.03)	29.87 (0.03)	26.22 (1.51)
House	16.46 (0.02)	25.68 (0.05)	27.42 (0.05)	27.49 (0.05)	29.46 (0.07)	25.69 (0.05)	26.26 (0.07)	29.64 (0.05)	33.29 (0.08)	27.69 (2.35)
Mandril	16.18 (0.01)	22.62 (0.01)	24.29 (0.01)	22.23 (0.01)	22.66 (0.02)	22.29 (0.03)	22.16 (0.03)	23.99 (0.02)	25.23 (0.02)	22.98 (1.06)
Peppers	16.40 (0.01)	24.87 (0.03)	26.29 (0.02)	25.94 (0.02)	26.82 (0.04)	24.86 (0.04)	25.05 (0.03)	27.64 (0.04)	29.33 (0.05)	26.07 (1.43)
Walk Bridge	16.41 (0.01)	22.08 (0.03)	23.57 (0.01)	21.87 (0.01)	22.38 (0.03)	21.83 (0.02)	21.99 (0.02)	23.61 (0.03)	24.26 (0.03)	22.53 (0.88)
Mean	16.50 (0.23)	22.65 (1.86)	24.13 (1.86)	22.68 (2.46)	23.81 (2.35)	22.49 (1.94)	22.84 (1.79)	25.32 (1.78)	26.59 (2.24)	23.57 (2.42)

Table 4 Denoising results in terms of SSIM for noise variance $\sigma^2 = 0.025$.

| Images	Noisy	Potts	NLPotts	GMRF	NLGMRF	GIMLL	NLGIMLL	NLM	BM3D	Mean (Std)
Swan	0.16 (0.00)	0.59 (0.00)	0.62 (0.00)	0.69 (0.00)	0.70 (0.00)	0.60 (0.00)	0.56 (0.00)	0.68 (0.00)	0.78 (0.00)	0.64 (0.07)
Sea Star	0.26 (0.00)	0.57 (0.00)	0.67 (0.00)	0.60 (0.00)	0.61 (0.00)	0.56 (0.00)	0.55 (0.00)	0.65 (0.00)	0.73 (0.00)	0.60 (0.06)
Eskimo	0.21 (0.00)	0.53 (0.00)	0.61 (0.00)	0.56 (0.00)	0.54 (0.00)	0.52 (0.00)	0.49 (0.00)	0.58 (0.00)	0.65 (0.00)	0.55 (0.05)
Bridge	0.24 (0.00)	0.50 (0.00)	0.55 (0.00)	0.52 (0.00)	0.58 (0.00)	0.50 (0.00)	0.48 (0.00)	0.60 (0.00)	0.68 (0.00)	0.54 (0.06)
Butterfly	0.28 (0.00)	0.60 (0.00)	0.68 (0.00)	0.64 (0.00)	0.67 (0.00)	0.60 (0.00)	0.58 (0.00)	0.70 (0.00)	0.79 (0.00)	0.64 (0.06)
Buildings	0.35 (0.00)	0.52 (0.00)	0.59 (0.00)	0.46 (0.00)	0.58 (0.00)	0.51 (0.00)	0.53 (0.00)	0.67 (0.00)	0.75 (0.00)	0.56 (0.08)
Boat and Bridge	0.21 (0.00)	0.49 (0.00)	0.54 (0.00)	0.52 (0.00)	0.54 (0.00)	0.49 (0.00)	0.46 (0.00)	0.58 (0.00)	0.66 (0.00)	0.52 (0.06)
Ostrich	0.12 (0.00)	0.57 (0.00)	0.57 (0.00)	0.78 (0.00)	0.74 (0.00)	0.60 (0.00)	0.53 (0.00)	0.63 (0.00)	0.83 (0.00)	0.64 (0.10)
Ships	0.40 (0.00)	0.47 (0.00)	0.55 (0.00)	0.45 (0.00)	0.55 (0.00)	0.46 (0.00)	0.48 (0.00)	0.66 (0.00)	0.78 (0.00)	0.53 (0.10)
Buildings and Boats	0.42 (0.00)	0.44 (0.00)	0.53 (0.00)	0.39 (0.00)	0.47 (0.00)	0.43 (0.00)	0.44 (0.00)	0.62 (0.00)	0.66 (0.00)	0.48 (0.09)
Castle	0.19 (0.00)	0.53 (0.00)	0.56 (0.00)	0.66 (0.00)	0.66 (0.00)	0.55 (0.00)	0.51 (0.00)	0.62 (0.00)	0.79 (0.00)	0.60 (0.08)
Horses	0.29 (0.00)	0.47 (0.00)	0.55 (0.00)	0.46 (0.00)	0.46 (0.00)	0.45 (0.00)	0.43 (0.00)	0.54 (0.00)	0.59 (0.00)	0.48 (0.05)
Miscellaneous	0.28 (0.00)	0.51 (0.00)	0.55 (0.00)	0.57 (0.00)	0.61 (0.00)	0.52 (0.00)	0.48 (0.00)	0.62 (0.00)	0.75 (0.00)	0.56 (0.08)
Rope	0.35 (0.00)	0.51 (0.00)	0.61 (0.00)	0.41 (0.00)	0.49 (0.00)	0.48 (0.00)	0.47 (0.00)	0.59 (0.00)	0.66 (0.00)	0.52 (0.07)
Corn	0.37 (0.00)	0.58 (0.00)	0.70 (0.00)	0.53 (0.00)	0.59 (0.00)	0.55 (0.00)	0.54 (0.00)	0.67 (0.00)	0.76 (0.00)	0.60 (0.08)
Dog	0.18 (0.00)	0.52 (0.00)	0.57 (0.00)	0.60 (0.00)	0.59 (0.00)	0.53 (0.00)	0.48 (0.00)	0.58 (0.00)	0.71 (0.00)	0.56 (0.06)
Zebra	0.28 (0.00)	0.50 (0.00)	0.56 (0.00)	0.53 (0.00)	0.55 (0.00)	0.50 (0.00)	0.47 (0.00)	0.62 (0.00)	0.70 (0.00)	0.54 (0.07)
Church	0.37 (0.00)	0.46 (0.00)	0.54 (0.00)	0.40 (0.00)	0.52 (0.00)	0.45 (0.00)	0.46 (0.00)	0.65 (0.00)	0.76 (0.00)	0.51 (0.10)
Taj Mahal	0.24 (0.00)	0.55 (0.00)	0.59 (0.00)	0.64 (0.00)	0.68 (0.00)	0.56 (0.00)	0.53 (0.00)	0.66 (0.00)	0.81 (0.00)	0.61 (0.08)
Woman	0.20 (0.00)	0.57 (0.00)	0.62 (0.00)	0.64 (0.00)	0.65 (0.00)	0.57 (0.00)	0.53 (0.00)	0.62 (0.00)	0.78 (0.00)	0.61 (0.07)
Jet Plane	0.18 (0.00)	0.61 (0.00)	0.64 (0.00)	0.74 (0.00)	0.75 (0.00)	0.63 (0.00)	0.57 (0.00)	0.69 (0.00)	0.85 (0.00)	0.67 (0.08)
Lake	0.24 (0.00)	0.57 (0.00)	0.64 (0.00)	0.64 (0.00)	0.65 (0.00)	0.58 (0.00)	0.54 (0.00)	0.65 (0.00)	0.76 (0.00)	0.61 (0.06)
Living Room	0.22 (0.00)	0.53 (0.00)	0.60 (0.00)	0.56 (0.00)	0.58 (0.00)	0.53 (0.00)	0.50 (0.00)	0.60 (0.00)	0.73 (0.00)	0.57 (0.07)
Pirate	0.19 (0.00)	0.56 (0.00)	0.62 (0.00)	0.63 (0.00)	0.62 (0.00)	0.56 (0.00)	0.52 (0.00)	0.61 (0.00)	0.73 (0.00)	0.59 (0.06)
Cameraman	0.16 (0.00)	0.59 (0.00)	0.62 (0.00)	0.73 (0.00)	0.76 (0.00)	0.62 (0.00)	0.56 (0.00)	0.66 (0.00)	0.84 (0.00)	0.66 (0.09)
Lena	0.15 (0.00)	0.58 (0.00)	0.62 (0.00)	0.73 (0.00)	0.70 (0.00)	0.60 (0.00)	0.55 (0.00)	0.64 (0.00)	0.82 (0.00)	0.64 (0.08)
House	0.11 (0.00)	0.62 (0.00)	0.64 (0.00)	0.82 (0.00)	0.81 (0.00)	0.65 (0.00)	0.58 (0.00)	0.68 (0.00)	0.90 (0.00)	0.70 (0.10)
Mandril	0.29 (0.00)	0.53 (0.00)	0.65 (0.00)	0.46 (0.00)	0.51 (0.00)	0.50 (0.00)	0.47 (0.00)	0.59 (0.00)	0.69 (0.00)	0.53 (0.08)
Peppers	0.16 (0.00)	0.56 (0.00)	0.59 (0.00)	0.69 (0.00)	0.67 (0.00)	0.58 (0.00)	0.53 (0.00)	0.63 (0.00)	0.76 (0.00)	0.61 (0.07)
Walk Bridge	0.31 (0.00)	0.50 (0.00)	0.60 (0.00)	0.45 (0.00)	0.48 (0.00)	0.47 (0.00)	0.46 (0.00)	0.57 (0.00)	0.61 (0.00)	0.51 (0.06)
Mean	0.25 (0.08)	0.54 (0.05)	0.60 (0.04)	0.58 (0.12)	0.61 (0.09)	0.54 (0.06)	0.51 (0.04)	0.63 (0.04)	0.74 (0.07)	0.58 (0.09)
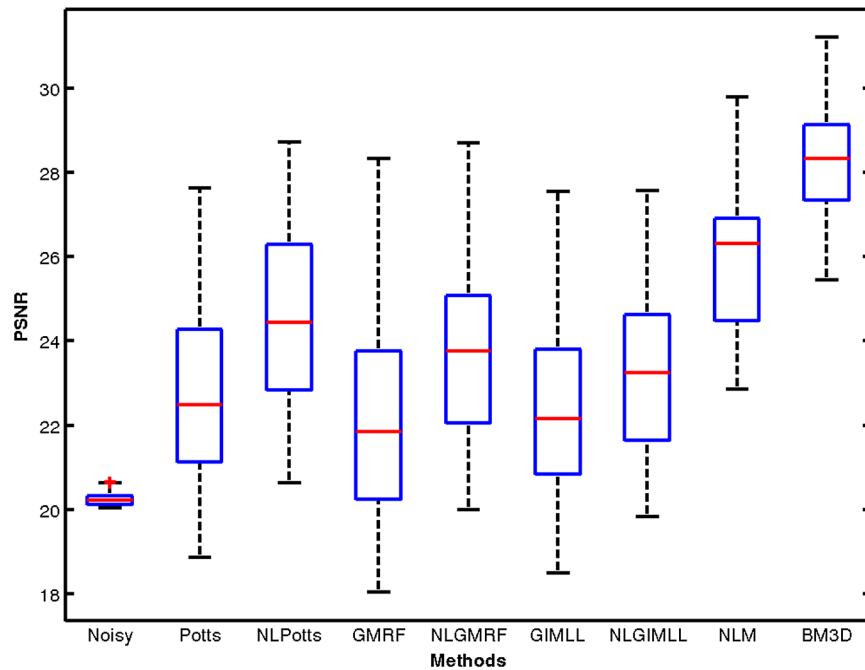
Fig. 14 Box plots of denoising results in terms of peak signal-to-noise ratio (PSNR) for Berkeley Database for noise variance $\sigma^2 = 0.010$ and h = 5.

So, the increase in the computational cost for our proposal is minimized.

In turn, two values of the smoothing parameter h for NLMRF models were tested here: $h = 3$ and $h = 5$. For search area W and patch P sizes 3×3 (i.e., eight neighbor patches or a second order-Markovian neighborhood) and 3×3, respectively, were used. It is important to emphasize that these parameters were not optimized.

Furthermore, the proposed methodology was compared against two state-of-the-art denoising methods for AWGN: NLM and BM3D. Basically, the complexity time for these methods is $\mathcal{O}(|W||N|\log|N|)$ and $\mathcal{O}(|N|)$ for NLM[36] and BM3D,[15] respectively, where $|W|$ is the size of the search area W. Thus, given that for the NLMRF models' calculation, the fast NLM method was used, the complexity time for each iteration of ICM with NLMRF models is
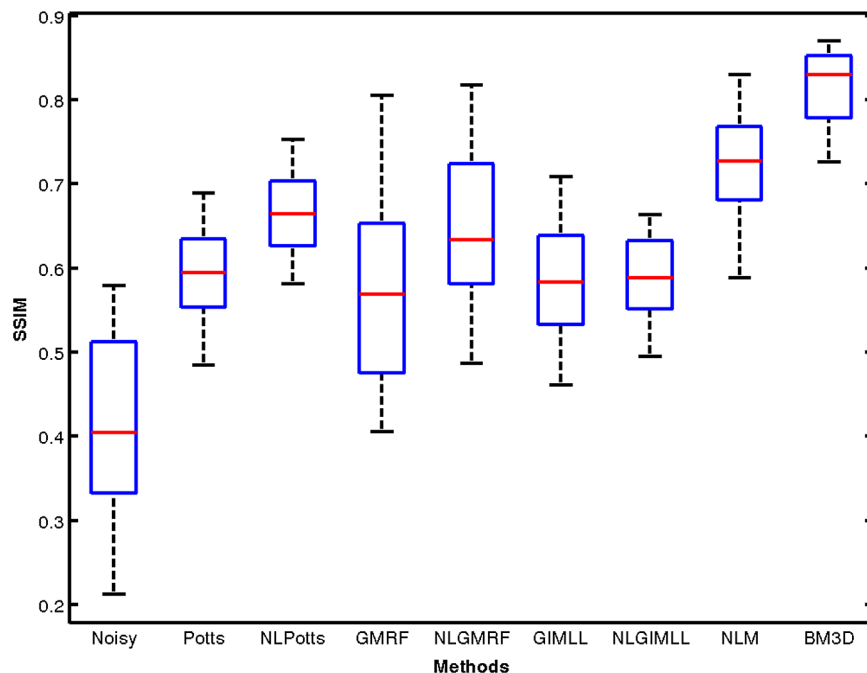
Fig. 15 Box plots of denoising results in terms of structural similarity index (SSIM) for Berkeley Database for noise variance $\sigma^2 = 0.010$ and h = 5.
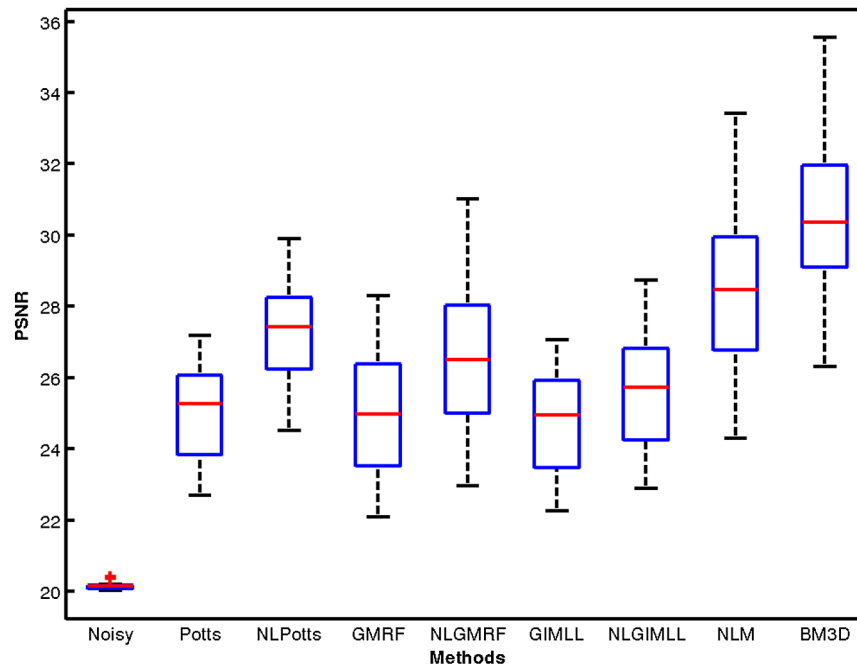
Fig. 16 Box plots of denoising results in terms of PSNR for Standard Database for noise variance $\sigma^2 = 0.010$ and $h = 5$.

$\mathcal{O}(|N| + |W||N| \log |N|) \propto \mathcal{O}(|W||N| \log |N|)$ in the case of only one weights estimation step or $\mathcal{O}(|W||N|^2 \log |N|)$ in the case of weights re-estimation.

Finally, the methodology was implemented in MATLAB (Fig. 3 summarizes the proposed methodology). The images used in the experiments were 10 images of Standard Database from USC-SPI (such as Jet Plane, Lena, Peppers, Lake, Pirate) and 20 images from the Berkeley segmentation dataset[37] (such as Castle, Rope, Dog, Buildings, Ships). For a better evaluation of the methods, for each original image used in this work, 10 noisy versions of them were generated by using 10 seeds of random noise.
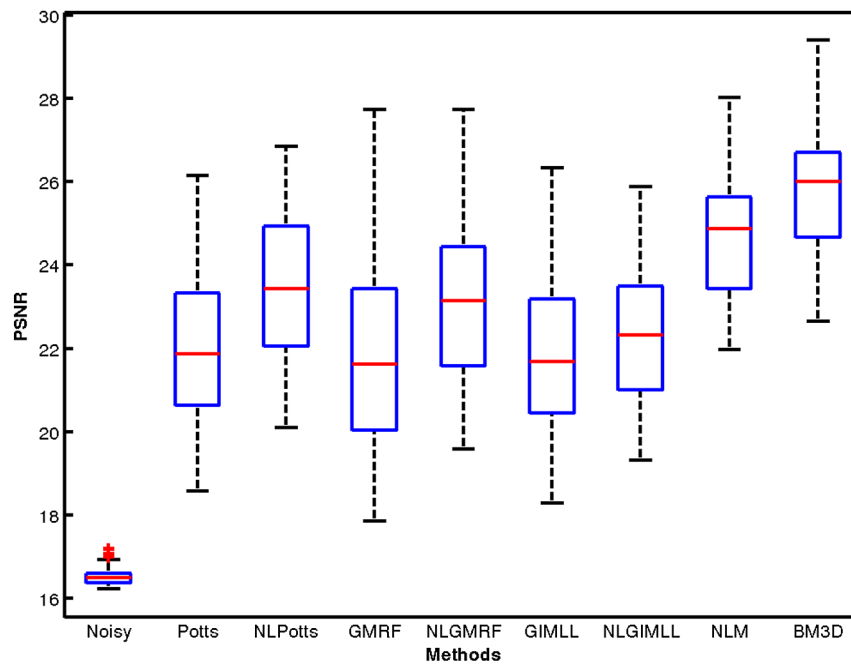
6 Results

By using the proposed experimental setup described previously, the denoising results for images corrupted by
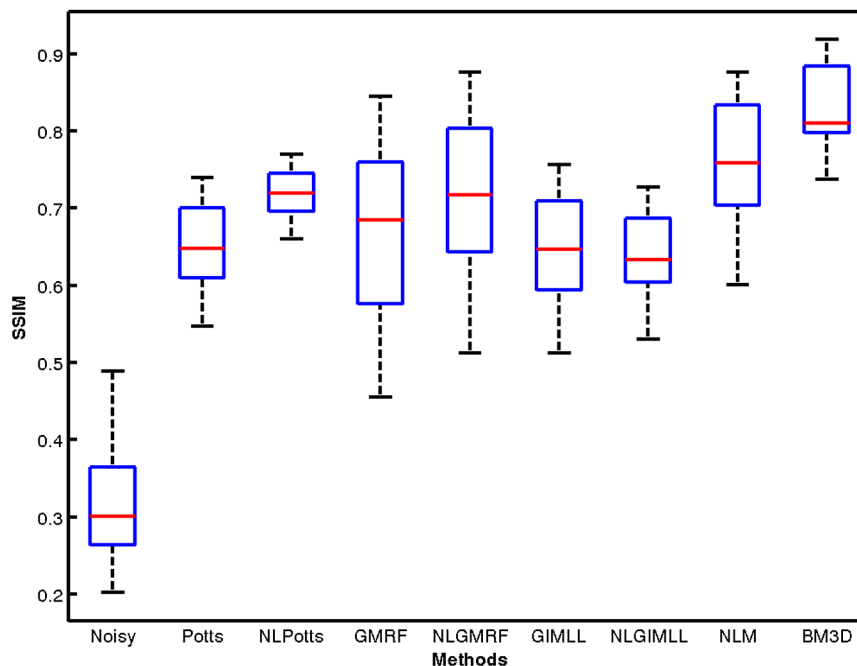
Fig. 17 Box plots of denoising results in terms of SSIM for Standard Database for noise variance $\sigma^2 = 0.010$ and $h = 5$.
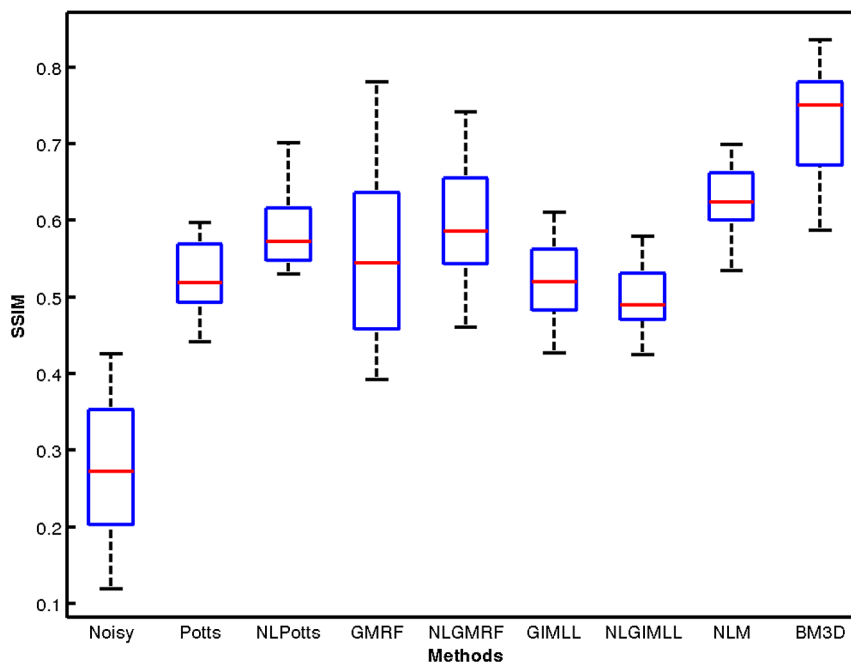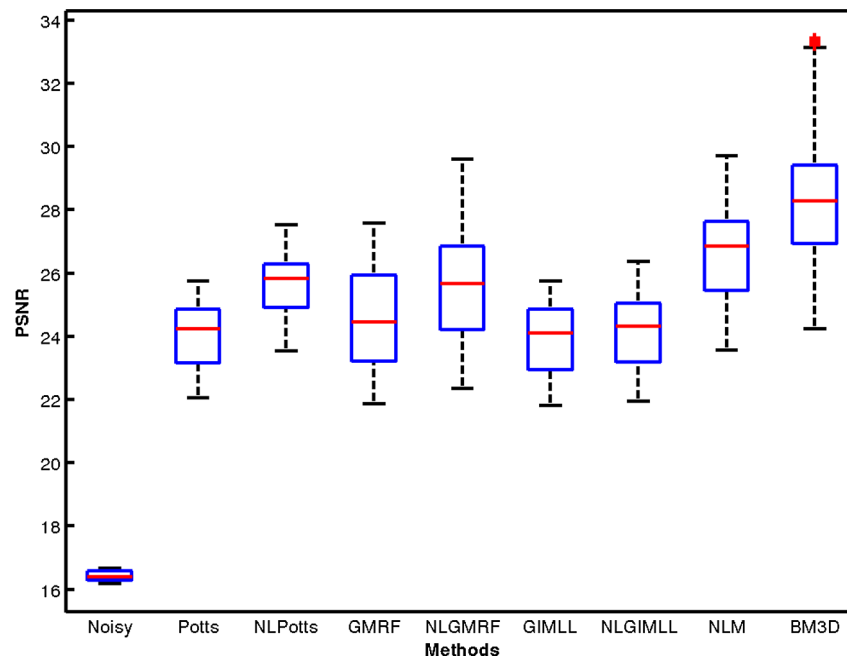
Fig. 18 Box plots of denoising results in terms of PSNR for Berkeley Database for noise variance $\sigma^2 = 0.025$ and $h = 5$.

Gaussian noise are presented and discussed in this section. The results can be found in Figs. 4–13 for visual analysis and in Tables 1–4 for a quantitative analysis in terms of peak signal-to-noise ratio (PSNR) and structural similarity index (SSIM)[38] measures, respectively. In addition, some box plots for each image database used here are displayed in Figs. 14–21 for further analysis.

In general, it can be observed from Tables 1–4 that the NLMRF models show considerably superior results in quantitative terms compared with their local versions. For instance, NLPotts, NLGMRF, and NLGIMLL achieved about 1.94, 1.51, and 0.83 dB on average higher than their local versions, with the noise variance $\sigma^2 = 0.01$, in terms of PSNR, respectively. For the noise variance

Fig. 19 Box plots of denoising results in terms of SSIM for Berkeley Database for noise variance $\sigma^2 = 0.025$ and $h = 5$.
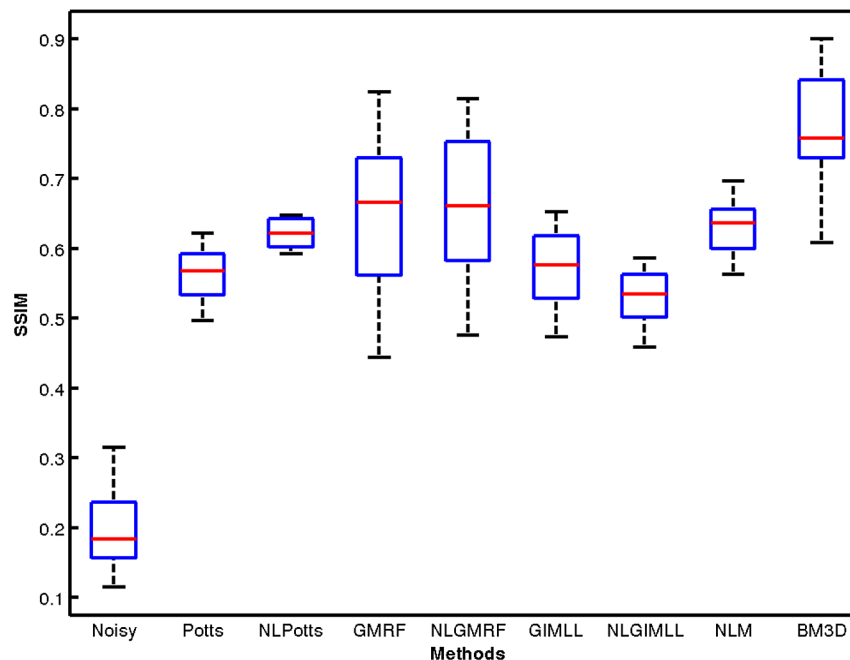
Fig. 20 Box plots of denoising results in terms of PSNR for Standard Database for noise variance $\sigma^2 = 0.025$ and $h = 5$.

$\sigma^2 = 0.025$, these values are 1.48, 1.13, and 0.35 dB, respectively.

In addition, there was also an improvement in terms of SSIM by using nonlocal Markovian models. For instance, NLPotts, NLGMRF, and NLGIMLL achieved about 0.07, 0.06, and 0.01 on average higher than their local versions, with the noise variance $\sigma^2 = 0.01$, respectively. For the noise variance $\sigma^2 = 0.025$, these values are 0.06, 0.03, and

−0.03, respectively. Note that there was a decrease for the NLGIMLL model. This can also be noted in the box plots in Figs. 19 and 21.

Although the BM3D filtering displayed the best results with all tested methods, NLGMRF and NLPotts models achieved the best results among all MRF models evaluated and were slightly higher in terms of SSIM than the NLM in some cases, mainly with higher values for the noise variance

Fig. 21 Box plots of denoising results in terms of SSIM for Standard Database for noise variance $\sigma^2 = 0.025$ and $h = 5$.

for Standard Database from USC-SIPI. This can be observed on box plots in Fig. 21.

Basically, the box plots of Figs. 14–21 summarize the achieved results of the methods in these experiments.

Finally, visual analysis of Figs. 4–13 seems to corroborate the quantitative results. It can be noted that the NLMRF models preserve the details better, mainly edges (see the results from images "Buildings" and "Ships" for a clear demonstration of this). Also, it can be noted that NLGMRF controls the smoothing better in comparison with GMRF (for instance, see the image "Jet Plane").

7 Conclusions and Future Works

In this paper, an extension of some classical MRF models was proposed by weighting the pairwise interaction of their energy functions. These weights are calculated as performed in the NLM method, where a similarity between nonlocal regions are calculated. Therefore, this paper proposed the following new nonlocal MRF model, namely, NLGMRF, NLPotts, and NLGIMLL. In addition, the MPLE of the spatial dependency parameter (β) for each of these models was also proposed.

These new models were applied as priors in an MAP–MRF framework for image denoising, achieving very good results and substantially increasing the quality of filtering. Thus, these NLMRF models were demonstrated to be more suitable for image denoising problems than their local/classical versions, improving the tradeoff between detail preservation and noise removal. In addition, obtaining this superior quality only slightly increased the complexity time, and was compatible to the NLM.

However, as the new models depend on the similarity measure used to determine the β weighting, a suitable smoothing parameter value needs to be estimated. This is the main limitation of these new models. Higher values for this parameter can oversmooth some regions of the images. This can also be observed in the results obtained by NLM.

In addition, a small search area size was used to obtain these results. This setup is defined to be compatible with the second-order Markovian neighborhood used in classical/local models. It is expected that the result can be increased by taking a bigger search area size, because more informative/similarity patches can be used for a better weights estimation.

Finally, future works include: (1) an automatic estimation of the smoothing parameter h in the weights calculation, (2) the evaluation of these new models for other image processing problems (such as image reconstruction and image segmentation), (3) the adaptation of these new models for other kinds of noise by using similarity measures suitable for each noise model as done for NLM in Ref. 28–30, (4) study of the parameter of search area size, and (5) extension to other MRF models.

References

1. M. Elad, M. Figueiredo, and Y. Ma, "On the role of sparse and redundant representations in image processing," *Proc. IEEE* **98**, 972–982 (2010).
2. P. Chatterjee and P. Milanfar, "Is denoising dead?," *IEEE Trans. Image Process.* **19**, 895–911 (2010).
3. D. T. Kuan et al., "Adaptive noise smoothing filter for images with signal-dependent noise," *IEEE Trans. Pattern Anal. Mach. Intell.* **7**(2), 165–177 (1985).
4. A. Buades, B. Coll, and J. M. Morel, "A review of image denoising algorithms, with a new one," *SIAM Multiscale Model. Simul.* **4**(2), 490–530 (2005).
5. B. Goossens et al., "An overview of state-of-the-art denoising and demosaicking techniques: toward a unified framework for handling artifacts during image reconstruction," in *International Image Sensor Workshop (IISW)* (2015).
6. P. Perona and J. Malik, "Scale-space and edge detection using anisotropic diffusion," *IEEE Trans. Pattern Anal. Mach. Intell.* **12**, 629–639 (1990).
7. L. Alvarez, P.-L. Lions, and J.-M. Morel, "Image selective smoothing and edge detection by nonlinear diffusion II," *SIAM J. Numer. Anal.* **29**(3), 845–866 (1992).
8. M. Black et al., "Robust anisotropic diffusion," *IEEE Trans. Image Process.* **7**, 421–432 (1998).
9. J. Weickert, *Anisotropic Diffusion in Image Processing*, Vol. 1, ECMI Series, Teubner-Verlag, Stuttgart, Germany (1998).
10. L. I. Rudin, S. Osher, and E. Fatemi, "Nonlinear total variation based noise removal algorithms," *Phys. D* **60**(1–4), 259–268 (1992).
11. A. Chambolle, "An algorithm for total variation minimization and applications," *J. Math. Imaging Vision* **20**(1–2), 89–97 (2004).
12. D. Donoho, "De-noising by soft-thresholding," *IEEE Trans. Inf. Theory* **41**, 613–627 (1995).
13. C. Tomasi and R. Manduchi, "Bilateral filtering for gray and color images," in *Sixth International Conference on Computer Vision (ICCV'1998)*, pp. 839–846 (1998).
14. S. Paris et al., "Bilateral filtering: theory and applications," *Found. Trends Comp. Graph. Vision* **4**(1), 1–73 (2008).
15. K. Dabov et al., "Image denoising by sparse 3-D transform-domain collaborative filtering," *IEEE Trans. Image Process.* **16**, 2080–2095 (2007).
16. E. Candes, J. Romberg, and T. Tao, "Robust uncertainty principles: exact signal reconstruction from highly incomplete frequency information," *IEEE Trans. Inf. Theory* **52**, 489–509 (2006).
17. J. Jin et al., "General image denoising framework based on compressive sensing theory," *Comp. Graph.* **38**, 382–391 (2014).
18. S. Geman and D. Geman, "Stochastic relaxation, Gibbs distributions, and the Bayesian restoration of images," *IEEE Trans. Pattern Anal. Mach. Intell.* **6**, 721–741 (1984).
19. S. Z. Li, *Markov Random Field Modeling in Image Analysis*, in Advances in Pattern Recognition, 3rd ed., Springer, London, UK (2009).
20. F.-C. Jeng and J. Woods, "Compound Gauss-Markov random fields for image estimation," *IEEE Trans. Signal Process.* **39**, 683–697 (1991).
21. D. H. P. Salvadeo, "Filtragem de Ruído em Imagens Tomográficas com Baixa Taxa de Contagem Utilizando uma Abordagem Bayesiana Contextual," PhD Thesis, Universidade Federal de São Carlos (2013) (in Portuguese).
22. G. Peyré, "A review of adaptive image representations," *IEEE J. Sel. Top. Signal Process.* **5**, 896–911 (2011).
23. Y. Chen et al., "Bayesian statistical reconstruction for low-dose X-ray computed tomography using an adaptive-weighting nonlocal prior," *Comp. Med. Imaging Graph.* **33**, 495–500 (2009).
24. Y. Chen et al., "PET transmission tomography using a novel nonlocal MRF prior," *Comp. Med. Imaging Graph.* **33**, 623–633 (2009).
25. M. Zhao et al., "Satellite image deconvolution based on nonlocal means," *Appl. Opt.* **49**, 6286–6294 (2010).
26. J. Sun and M. Tappen, "Learning non-local range Markov random field for image restoration," in *IEEE Conference on Computer Vision and Pattern Recognition (CVPR 2011)*, pp. 2745–2752 (2011).
27. C. S. Won and R. M. Gray, *Stochastic Image Processing, Information Technology: Transmission, Processing, and Storage*, Kluwer Academic/Plenum Publishers, New York (2004).
28. C. Deledalle, "Image denoising beyond additive Gaussian noise patch-based estimators and their application to SAR imagery," PhD Thesis, Télécom ParisTech (2011).
29. C. Deledalle, L. Denis, and F. Tupin, "How to compare noisy patches? patch similarity beyond gaussian noise," *Int. J. Comp. Vision* **99**, 86–102 (2012).
30. C. Deledalle, L. Denis, and F. Tupin, "Iterative weighted maximum likelihood denoising with probabilistic patch-based weights," *IEEE Trans. Image Process.* **18**, 2661–2672 (2009).
31. J. Besag, "Statistical analysis of non-lattice data," *J. R. Stat. Soc.* **24**(3), 179–195 (1975).
32. A. L. M. Levada, N. D. A. Mascarenhas, and A. Tannús, "Pseudolikelihood equations for Potts MRF model parameter estimation on higher order

neighborhood systems," *IEEE Geosci. Remote Sens. Lett.* **5**, 522–526 (2008).

33. A. Martins et al., "MAP-MRF super-resolution image reconstruction using maximum pseudo-likelihood parameter estimation," in *16th IEEE Int. Conf. on Image Processing (ICIP 2009)*, pp. 1165–1168 (2009).
34. J. Besag, "On the statistical analysis of dirty pictures," *J. R. Stat. Soc. Ser. B* **48**(3), 259–302 (1986).
35. R. Brent, *Algorithms for Minimization without Derivatives*, Prentice-Hall, Englewood Cliffs, New Jersey (1973).
36. C. Deledalle, V. Duval, and J. Salmon, "Non-local methods with shape-adaptive patches (NLM-SAP)," *J. Math. Imaging Vision* **43**, 103–120 (2012).
37. P. Arbelaez et al., "Contour detection and hierarchical image segmentation," *IEEE Trans. Pattern Anal. Mach. Intell.* **33**, 898–916 (2011).
38. Z. Wang and A. C. Bovik, "Mean squared error: love it or leave it? a new look at signal fidelity measures," *IEEE Signal Process. Mag.* **26**, 98–117 (2009).

Denis H. P. Salvadeo received his BSc, MSc, and PhD in computer science from the Federal University of São Carlos (UFSCar), São Carlos, Brazil, in 2007, 2009, and 2013, respectively. He is currently a professor of computer science at São Paulo State University (UNESP), Rio Claro, Brazil. His research interests include digital image processing, computer vision, medical images, random field models, and nonlocal approaches.

Nelson D. A. Mascarenhas received his BSc and MSc in electronic engineering from the Technological Institute of Aeronautics, São José dos Campos, Brazil, in 1966 and 1969 and a PhD in electrical engineering from the University of Southern California in 1974. He is presently associated with Faculdade Campo Limpo Paulista, Brazil. His research interests are in digital image processing and pattern recognition.

Alexandre L. M. Levada received his BSc degree in computer science from São Paulo State University (UNESP) in 2002, MSc degree in computer science from Federal University of São Carlos (UFSCar) in 2006, and PhD degree in computational physics from São Paulo University (USP) in 2010. He is a professor of computer science at Federal University of São Carlos, SP, Brazil. His research interests include pattern recognition, image processing, and random field models.